Surface Modification of AMH-3 for Development of Mixed Matrix Membranes

by

Elaine Chong Nyuk Tzi

16791

Dissertation submitted in partial fulfillment of
the requirements for the
Bachelor of Engineering (Hons)
(Chemical Engineering)

MAY 2015

Universiti Teknologi PETRONAS
32610 Bandar Seri Iskandar
Perak Darul Ridzuan

CERTIFICATION OF APPROVAL

Surface Modification of AMH-3 for

Development of Mixed Matrix Membranes

by

Elaine Chong Nyuk Tzi

16791

A project dissertation submitted to the
Chemical Engineering Programme
Universiti Teknologi PETRONAS
in partial fulfillment of the requirements for the
BACHELOR OF ENGINEERING (Hons)
(CHEMICAL ENGINEERING)

Approved by,

_____
(Dr. Oh Pei Ching)

UNIVERSITI TEKNOLOGI PETRONAS
BANDAR SERI ISKANDAR, PERAK
May 2015

CERTIFICATION OF ORIGINALITY

This is to certify that I am responsible for the work submitted in this project, that the original work is my own except as specified in the references and acknowledgements, and that the original work contained herein have not been undertaken or done by unspecified sources or persons.

_____

ELAINE CHONG NYUK TZI

ABSTRACT

AMH-3 layered silicate is chosen for this study as its 3D structure with crystallographic pore size of 3.4 Å makes it an attractive material for gas separation applications. AMH-3 layered silicate was synthesized via hydrothermal synthesis method and then functionalized using octyl(methyl)dimethoxysilane to enhance its hydrophobicity for good adhesion and dispersion in mixed matrix membrane. In this work, high permeability polysulfone (PSf) was incorporated with AMH-3 for fabrication of mixed matrix membranes. The critical polymer concentration of PSf was studied to suppress the formation of macrovoids in mixed matrix membranes. Flat sheet PSf/AMH-3 membranes were then prepared by dry/wet phase inversion technique with different loadings of AMH-3 in PSf matrix. The synthesized AMH-3 layered silicate is verified by FT-IR and XRD analysis. Structural changes of AMH-3 after functionalization are observed in FT-IR, XRD and SAP analysis. Functionalized AMH-3 shows higher surface area and reduced pore size. The MMMs of pristine and functionalized AMH-3 have similar surface and cross-sectional morphologies, showing good distribution and dispersion of inorganic filler. AMH-3 shows improved hydrophobicity after functionalization, resulting in better adhesion and compatibility with polysulfone.

ACKNOWLEDGEMENT

First and foremost, I would like to thank God for His provision of strength and wisdom in completing this final year project.

I owe a debt of thanks to my supervisor, Dr. Oh Pei Ching for her professional guidance, enthusiastic support and useful critiques throughout the entire project. Her constructive advices and encouragement have greatly increased my understanding and interest in the area of this project. I am truly grateful to have a helpful supervisor who taught me to be resourceful and also financially supported the project with her research grant.

I would like to extend my appreciation to the UTP staffs including the laboratory technologists in Chemical Engineering department, Central Analytical Laboratory and Mechanical Engineering department for their assistance and cooperation. Also, I would like to thank the MTDC Lab, School of Chemical Engineering Universiti Sains Malaysia, for the permission to use the contact angle goniometer.

My heartfelt gratitude goes to my parents, family members and friends for their love and support.

TABLE OF CONTENTS

LIST OF FIGURES

LIST OF TABLES

CHAPTER 1

INTRODUCTION

1.1 Background

Natural gas has emerged as an important energy resource due to the increasing attention and demand to seek more environmental friendly fuel sources. Methane is the primary component of natural gas accompanied by other light alkanes and impurities. Table 1.1 shows the chemical composition of Malaysia crude natural gas, analysed using gas chromatography-mass spectroscopy (Abu Bakar *et al.*, 2012). High content of impurities including carbon dioxide (CO_2) and hydrogen sulphide (H_2S) contribute to sour natural gas and the purification process known as natural gas sweetening is necessary to remove the acid gases.

TABLE 1.1 Chemical Composition of Crude Natural Gas from Telaga Bergading, PETRONAS Carigali Sdn. Bhd.

Gases	Composition (%)
CH_4	47.0
CO_2	23.5
H_2S	5.4
Others (CO, O_2, N_2)	24.1

Carbon dioxide, one of the major contaminants in natural gas is also a prominent greenhouse gas contributing to global climate change. The presence of CO_2 reduces the energy content and compressibility of natural gas and thus affects the selling price of the natural gas. Furthermore, CO_2 in the natural gas stream is acidic and corrosive in the presence of water and subsequently contributes to the corrosion of equipment and transport pipelines (Zhang *et al.*, 2013). While cooling down natural gas to low temperature, the carbon dioxide freezes and blocks pipelines and causes

difficulties in transportation. Thus, CO_2 concentration of 2% and below is required to meet the typical pipeline specifications for natural gas (Othman *et al.*, 2009).

Therefore, the separation of CO_2 from CH_4 is necessary and various technologies have been employed for natural gas purification including absorption, adsorption, cryogenic, and membrane process. Membrane technology has shown promising features of energy efficiency, simplicity of operation, economical processability and separation performance.

1.2 Problem Statement

Membranes have been extensively used in gas separation. Polymeric membrane possesses high economical processability and good mechanical properties. However, the limitation of trade-off between permeability and selectivity restrained the gas separation performance of the polymeric membrane. On the other hand, inorganic membrane exhibits high chemical and thermal stability, high permeability and selectivity but requires high cost.

This leads to the development of mixed matrix membranes (MMMs) which combines the advantage of both types of membrane. MMMs comprising of molecular sieve materials embedded in a polymer matrix, are expected to exhibit improved gas separation performance and economically viable. However, poor interfacial contact between polymer and inorganic filler results in the formation of voids and subsequently deteriorates the membrane separation performance (Bakhtiari & Sadeghi, 2014).

Generally, polymeric membrane has high hydrophobic characteristic while layered silicate such as AMH-3 has strong hydropilicity due to the cations between the layers (Tsapatsis *et al.*, 2005). Therefore, the surface modification of layered silicate is necessary in order for the inorganic filler to be compatible with the polymeric matrix.

1.3 Objectives and Scope of Study

1. To synthesize AMH-3 layered silicate via hydrothermal synthesis method
2. To modify AMH-3 layered silicate by silane condensation method
3. To fabricate PSf/AMH-3 mixed matrix membranes (MMMs) using dry-wet phase inversion method
4. To characterize the AMH-3 particles and MMMs by using various analytical tools

1.4 Relevancy and Feasibility

Mixed matrix membrane (MMM) is an emerging technology for gas separation applications. There is a continuous ongoing process of selecting the best pair of polymeric and inorganic materials for MMM with better separation performances. Thus, this research project is highly relevant as the focus on the project is to synthesize and modify the inorganic filler for fabrication of MMM.

The proposed project is subjected to completion within a time frame of 28 weeks. A feasible and detailed plan with specific time allocated for each part of the whole project are determined. All chemicals and equipment needed are available in the laboratory and the characterization equipment are available in the university.

TABLE 1.2 Estimated Time Required for Each Experimental Task

Task	Duration (hours)	Duration (days)
Synthesis and purification of AMH-3	78	
Swelling and functionalization of AMH-3	43	
Fabrication of MMM	90	
TOTAL	211	9

The experiments can be carried out concurrently which would significantly reduce the total time required for the experimental works. Therefore, this research is feasible within the scopes identified and the time allocated.

CHAPTER 2

LITERATURE REVIEW

2.1 Gas Separation Technology

Various technology have been developed for removal of CO_2 from natural gas including absorption, adsorption, cryogenic distillation and membrane. Figure 2.1 summarizes the current gas separation technologies.

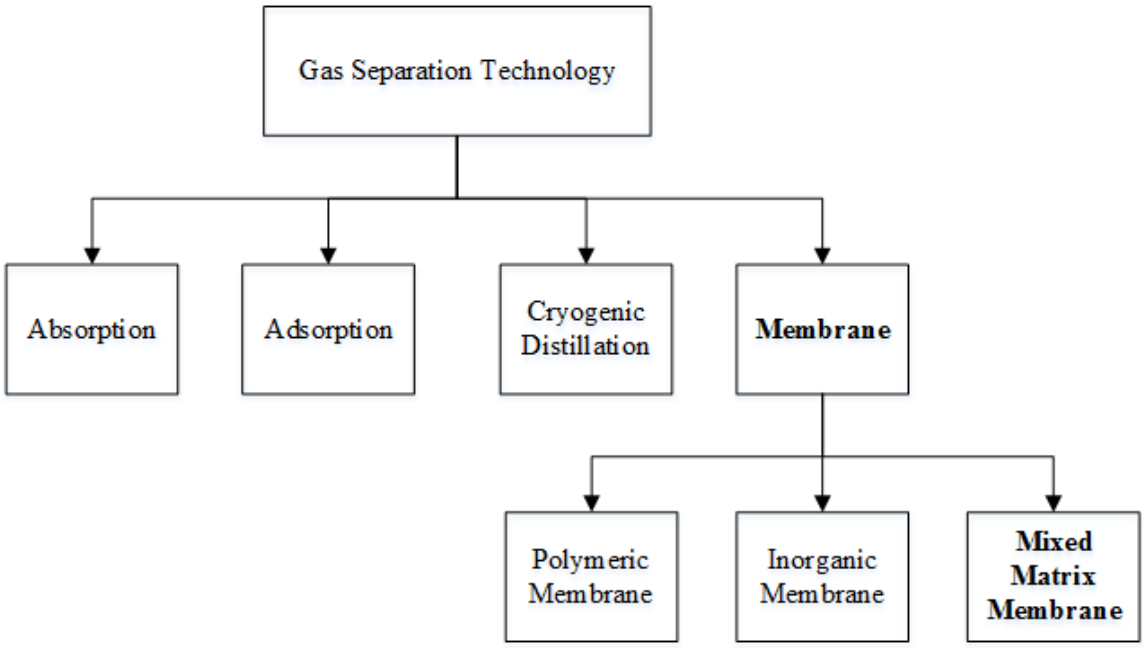

FIGURE 2.1 Summary of Gas Separation Technologies

2.1.1 Absorption

Absorption is a process where the gas mixture is contacted with the selective solvent in a plate or packed column. Absorption process is classified into physical and chemical absorption based on the interaction of the solvent and the absorbed gas component. Physical absorption occurs when the desired gas component is more soluble in the solvent compared to other components in the gas phase. On the other hand, for chemical absorption, the gas component forms weakly bonded intermediate compound with the solvent. The solvent requires regeneration after reaching its saturation level by heating or pressure reduction (Shimekit & Mukhtar, 2012).

Chemical absorption process using amine solutions is one of the state of art technology implemented industrial process. The common amine based solvents utilized for the absorption process includes monoethanolamine (MEA), diethanolamine (DEA), diglycolamine (DGA) and methyldiethanolamine (MDEA) (Rufford *et al.*, 2012).

Some of the major disadvantages of current amine absorption technology includes amine regeneration requires large amount of energy, equipment corrosion by amine solutions and solvent degradation problems in the presence of oxygen (Fryxell & Cao, 2012).

2.1.2 Adsorption

Adsorption is defined as the adhesion of the gas components on the surface of solid adsorbent. Activated carbons, silica gel, ion-exchange resins, zeolites, meso-porous silicates, activated alumina, metal oxides, and other surface-modified porous media are the conventional adsorbents used for adsorption process (Li *et al.*, 2011).

Regeneration of the adsorbent by desorption of the adsorbed gas is important as it may affect its adsorption capacity. Typical adsorption process is performed by looping in two beds of adsorbents simultaneously where one bed adsorbs and the second bed desorbs at the same time. Since the adsorption equilibrium is given by specific operating conditions (composition, temperature and pressure), the adsorbent can be regenerated by changing one of the process parameters. The two common industrial adsorption process for gas separation are pressure swing adsorption (PSA) and temperature swing adsorption (TSA).

In PSA, the gas mixture flows through a packed bed of adsorbent at elevated pressure until the concentration of the desired gas approaches equilibrium. The bed is regenerated by reducing the pressure and thereby releasing the selectively adsorbed components. As in TSA, the adsorbent is regenerated by raising its temperature (Kenarsari *et al.*, 2013). TSA is energy and time consuming due to the repeated heating and cooling process whereas PSA requires high operating cost for high pressure process.

2.1.3 Cryogenic Distillation

Cryogenic distillation uses a principle of separation based on cooling and condensation, and has been used in liquid separations for a long time. In the conventional cryogenic separation process, n-butane is added into the condenser of the distillation column to prevent solidification of carbon dioxide (Holmes *et al.*, 1982).

Cryogenic separation is widely used commercially for streams with high CO_2 concentrations (typically >90%) but it is not practical to be used for more dilute CO_2 streams (Kenarsari *et al.*, 2013). Cryogenic separation is able to produce natural gas of pipeline-quality, directly from sour gas stream.

One major drawback of cryogenic separation of CO_2 is the massive amount of energy required to provide the refrigeration necessary for the process, particularly for dilute gas streams. Also, some components such as water, have to be removed before the gas stream is cooled, to avoid blockages (Xu *et al.*, 2014).

2.1.4 Membrane

A membrane acts as a physical barrier which is capable of separating molecular mixture selectively by allowing certain compounds to pass through depending on their physical or chemical properties. The components that pass through are known as permeate whereas the retained solute is the retentate. Figure 2.2 illustrates the membrane separation principle (Schmeling *et al.*, 2010).

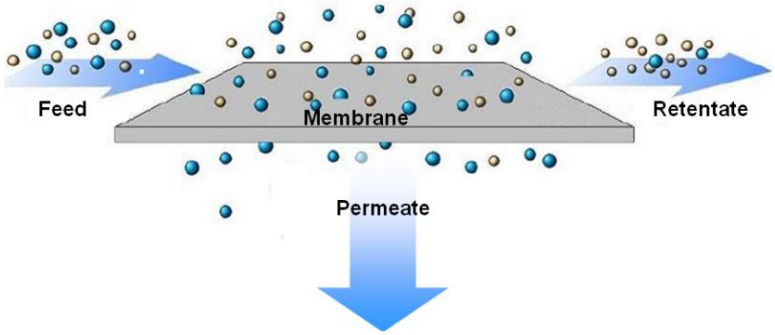

FIGURE 2.2 Principle of Membrane Separation

Initially, membranes and membrane processes were employed as analytical tool in chemical and biomedical laboratories (Elvers *et al.*, 2003). The technology eventually developed rapidly into industrial applications in various fields such as chemicals processing, food industry, gas separation, water purification, pharmaceutical industry, medical use and wastewater treatment.

Due to the transport selectivity of the membrane, the application of membrane technology in gas separation developed vastly in recent years. Furthermore, membrane processes are typically more energy efficient, easy to operate and scale up and have low environmental impact.

The driving force of membrane operation for gas separation is the pressure difference. Permeability and selectivity are the key factors in membrane transport performance (Sanders *et al.*, 2013). Permeability is a measure of the volume of gas the membrane can process while selectivity is a measure of the membrane's ability to separate components. The success of the membrane unit operation is also influenced by other factors such as chemical, thermal and mechanical stability, fouling tendencies, working lifetime, production costs and modularity (Rufford *et al.*, 2012).

Permeability (P) = Solubility (S) x Diffusivity (D)

For an ideal binary mixture, the selectivity is defined as

$$\alpha_{A/B} = P_A / P_B \quad (1)$$

Where

P_A permeability of component A

P_B permeability of component B

The typical unit for permeability is Barrer (Stern, 1968).

$$1\ Barrer = 10^{-10} \frac{cm^3(STP) \cdot cm}{cm^2 \cdot cmHg \cdot s}$$

2.2 Polymeric Membrane

The major membrane materials for gas separation technologies are polymers due to their easy processability with asymmetric structures, good mechanical properties, low cost and ease of operation (S. Kim & Lee, 2013). The common polymer materials employed to fabricate polymeric membrane includes cellulose acetate (CA), polyimide (PI), polycarbonates (PC), polyethersulfone (PES), and polysulfone (PSf) (Zhang *et al.*, 2013). These polymers exhibits a variety of structural and dynamical behavior which results in wide range of molecular permeation properties (W.-g. Kim & Nair, 2013).

The solution-diffusion model is the most widely used to describe the transport mechanism for gas permeation in polymeric membrane. The permeants first dissolve in the membrane material and then diffuse through the membrane down a concentration gradient. A separation is achieved between different permeants due to the differences in the amount of material that dissolves in the membrane and the rate of the material diffusing through the membrane (Wijmans & Baker, 1995). According to the model, the diffusivity coefficient and the solubility coefficient are the two dominant parameters controlling the permeation of molecules through membranes (T.-S. Chung *et al.*, 2007).

The intrinsic trade-off relationship between selectivity and permeability which is known as Robeson's upper bound limit, has become a significant limitation in industrial applications of polymeric membranes (Robeson, 2008). The inverse relationship is where higher permeability polymeric membrane are usually less selective and vice versa. The revisited upper bound relationship by Robeson for CO_2/CH_4 separation is illustrated in Figure 2.3 (Robeson, 2008). Table 2.1 shows the separation performance of polymeric membranes for CO_2/CH_4.

Furthermore, most polymeric membranes are susceptible to high temperatures and chemical degradation. Some polymers tend to swollen or plasticized when exposed to hydrocarbons or CO_2 at high partial pressure (Brunetti *et al.*, 2010). The CO_2 – induced plasticization is a phenomenon where CO_2 permeability increases with pressure but the selectivity declines (Ismail & Lorna, 2002). Plasticization is a swelling of the membrane structure due to sorption of a penetrant within the polymer matrix. It generally leads to an increase in the fractional free volume of the membrane which

increases the diffusion of all gas species through the membrane (Kentish, 2011). This results in an increase in permeability but a loss of selectivity and the loss of mechanical strength Thus, the performance of the polymeric membrane deteriorates significantly and the membrane is susceptible to failure (Scholes *et al.*, 2010).

On the other hand, ageing of membrane is the reverse of plasticization. It is the compaction of membrane structure over time and leads to loss of fractional free volume (Kentish, 2011). As a result, the permeability of the membrane decreases while the selectivity increases.

Therefore, the use of polymeric membranes in gas separation are still limited due to the low gas separation performance of the existing polymeric materials coupled with their poor chemical and thermal stabilities.

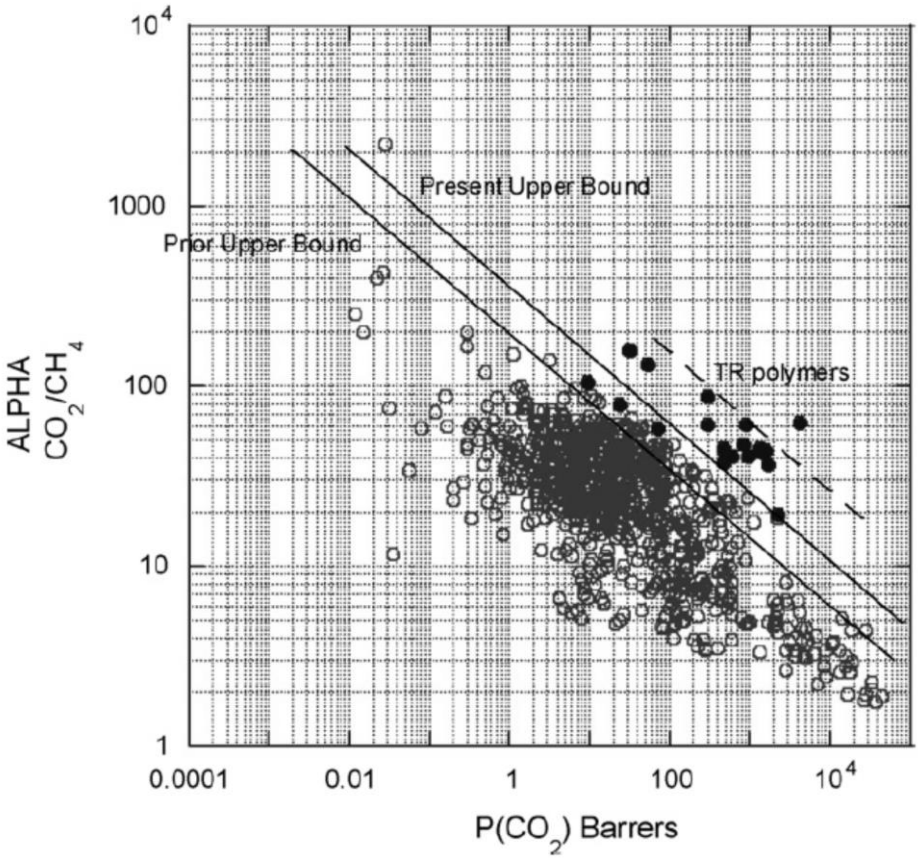

FIGURE 2.3 Upper Bound Correlation for CO_2/CH_4 Separation

Polymeric membrane is commonly prepared by phase inversion technique. It can be described as a demixing process whereby a homogeneous polymer solution is converted from liquid to solid state in a controlled manner. The most widely used phase inversion technique is the immersion precipitation. The polymer solution is casted on a supporting layer and immersed in a non-solvent coagulation bath (typically water). The solvent exchange between polymer solution and non-solvent coagulation bath results in precipitation and solidification of polymer film (Lalia *et al.*, 2013).

Pinnau and Koros (1993) introduced the dry/wet phase inversion technique for fabrication of ultra-thin defect free membrane. The cast film is subjected to convective and free standing evaporation prior to immersion in coagulation bath. The convective evaporation step is crucial to produce ultra-thin defect free asymmetric membrane.

Most of the industrialized membranes are asymmetric in structure which have high permeability and good mechanical strength. It is formed by two layers consisting of a very thin dense top layer, porous sublayer at the bottom. The permeation properties of the membrane is determined by the top dense layer while the porous sublayer only provides mechanical support to the membrane (Khulbe *et al.*, 2007).

The membrane morphologies and performances rely on many experimental parameters, including polymer concentration, type of solvent and non-solvent, condition of membrane casting and solvent exchange conditions (Hołda *et al.*, 2013). Polymer concentration has been identified as one of the most influential parameters on the membrane performance and morphology (Yampolskii, 2011). Preparation of the polymer membranes with different concentrations is a method for optimizing the effect of the polymer concentration but it is costly and time-consuming (Shamsabadi *et al.*, 2013). Therefore, viscometric test can be carried out to determine the optimum concentration of PSf for fabrication of mixed matrix membranes.

Formation of macrovoids is an unfavorable common defect in solution-cast membranes. Macrovoids jeopardize the mechanical integrity of a polymeric membrane support by acting as sites of increased local stress (McKelvey & Koros, 1996). Peng *et al.* (2008) suggested that the formation of macrovoids can be suppressed at a critical polymer concentration.

TABLE 2.1 CO_2/CH_4 Separation Performance of Polymeric Membrane

Membrane Material	**Pressure (bar)**	**Temperature (°C)**	**CO_2 Permeability**		**Selectivity (CO_2/CH_4)**	**Reference**
			Value	**Unit**		
Cellulose acetate (CA)	8	35	2.5	GPU	20.0	Visser *et al.* (2007)
Polybenzimidazole (PBI)	20	35	0.16	Barrer	89.0	Kumbharkar *et al.* (2006)
Polycarbonate (PC)	20	30	2.0	Barrer	27.2	Sridhar *et al.* (2007)
Polyetherimide (PEI)	15	25	0.76	GPU	43.1	Hashemifard *et al.* (2011)
Polysulfone (PSf)	4	35	6.3	Barrer	29.0	Ahn *et al.* (2008)

2.3 Inorganic Membrane

Various types of inorganic materials are used to synthesize membranes for gas separation which include ceramic (eg. silica, zeolite), metal organic frameworks, carbon, ionic liquids and amorphous metal oxides. Inorganic membranes are generally categorized into two groups based on their structure which are the dense membrane and porous membrane. Porous inorganic membranes vary greatly in pore size, support material, and configuration. They usually exhibit higher permeability compared to polymeric membranes. On the other hand, dense inorganic membranes are very specific in their separation behaviours and usually show lower permeability (Ismail & David, 2001).

Inorganic membranes offer high thermal and chemical stability, high mechanical strength and high separation performances (Rezakazemi *et al.*, 2014). Besides that, inorganic membranes have higher throughput and longer lifespan compared to polymeric membrane.

However, large scale fabrication of inorganic membrane is laborious and costly due to its fragile structure and low surface-to-volume ratio (Koros, 2002). Also, difficulty in preparing defect-free membrane also hindered the large scale implementation of inorganic membrane.

2.3.1 Layered Silicate

Layered silicates are inorganic materials that are naturally layered in structure and the layers are usually separated by gallery space which is occupied by water molecules and alkaline-earth metal cations. Typically, their basic building blocks are tetrahedral sheets in which silicon is surrounded by four oxygen atoms, and aluminium octahedral sheets (Pavlidou & Papaspyrides, 2008).

The layer thickness is around 1 nm and the lateral dimensions may vary from 300 Å to several microns, and even larger, depending on the particulate silicate, the source of the clay and the method of preparation. Some of the properties of layered silicates include high cation-exchanged capacities, large surface area, high surface reactivities and adsorptive properties (Tsapatsis *et al.*, 2005).

Layered silicates are found in both natural clays and synthetic minerals. Some of the common natural layered silicates are montmorillonite (MMT), hectorite and kaolinite. On the other hand, a few synthetic layered silicates that are developed in recent years include MCM-22 and AMH-3. Table 2.2 lists some of the properties of AMH-3 and MCM-22 layered silicate.

TABLE 2.2 Properties of AMH-3 and MCM-22

	AMH-3	**MCM-22**
Chemical Structure	$Na_8Sr_8Si_{32}O_{76} \cdot 16H_2O$	$[H^+_{2.4}Na^+_{3.1}][Al_{0.4}B_{5.1}Si_{66.5}O_{144}]$
Pore Structure	8 membered ring	10 membered ring
Structure (Dimension)	3D	2D
Pore Aperture (Å)	3.4	5.4 × 4.0

2.4 Mixed Matrix Membrane

Mixed matrix membranes (MMM) are hybrid membranes formed by incorporating dispersed inorganic fillers into continuous polymer matrix. Figure 2.4 illustrates the schematic of a MMM (T.-S. Chung *et al.*, 2007). The bulk phase represented by phase A is the polymer matrix while phase B is the dispersed inorganic fillers.

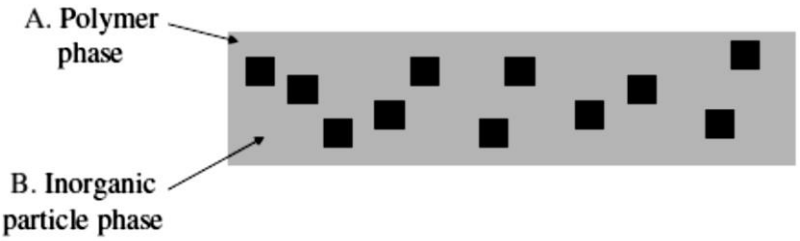

FIGURE 2.4 Schematic Diagram of a Mixed Matrix Membrane

Mixed matrix membrane is introduced with the aim of overcoming the limitations of polymeric and inorganic membranes. It offers the potential to achieve good adhesion properties between organic and inorganic composite, improved gas separation performance and enhanced mechanical properties of conventional polymeric membrane (Ahmad *et al.*, 2012). Table 2.3 summarizes the comparison of properties between polymeric membrane, inorganic membrane and mixed matrix membrane.

The gas transport performance of mixed matrix membrane is altered by various factors including the properties of polymer and inorganic materials, the compatibility of the materials, morphology and the membrane formation process (Ahn *et al.*, 2008).

The dominant mechanism in MMMs is the combination of the solution diffusion and Knudsen diffusion (Rezakazemi *et al.*, 2014). The effective permeability of the MMM can be calculated using the Maxwell model, as shown in equation 2 (Noble, 2011). This equation is valid for spherical particles in dilute suspensions where the interaction between the particles is negligible.

$$P_{eff} = P_c \left[\frac{P_d+2P_c-2\emptyset_d(P_c-P_d)}{P_d+2P_c+\emptyset_d(P_c-P_d)}\right] \quad (2)$$

Where

P_{eff} effective permeability of the MMM

P_c permeability of the continuous polymer phase

P_d permeability of the dispersed inorganic phase

$\emptyset_d$ volume fraction of the dispersed phase

Various combinations of polymer and inorganic materials have been studied in the recent years as different combinations results in different gas separation performances. The inorganic fillers used in MMMs are mostly porous molecular sieve type materials as this generally leads to higher permeability and selectivity in MMMs (Hashemifard *et al.*, 2011). In many cases, the selectivity is significantly improved by addition of a small amount of molecular sieves to the polymeric matrix (Rezakazemi *et al.*, 2014).

Choi, Coronas, Lai*, et al.* (2008) made a comparison on the performance of mixed matrix membranes incorporating MCM-22, proton exchanged AMH-3 (PAMH), and swollen AMH-3 (SAMH) respectively into polybenzimidazole (PBI) matrix. Both PBI/PAMH and PBI/PSAMH mixed matrix membranes presented significantly improved selectivity for H_2/CO_2 separation compared to pure PBI membranes. On the other hand, PBI/MCM-22 did not show improvement on selectivity for H_2/CO_2 separation (Choi, Coronas, Lai*, et al.*, 2008).

One of the major problems in the making of MMM is the inorganic material agglomeration. Ideally, the dispersed inorganic phase should be evenly distributed in the continuous polymer phase. Overloading of inorganic fillers will result in the agglomeration of inorganic fillers in the MMM and subsequently reduces the gas permeability (Khan *et al.*, 2012). Therefore, an optimum loading of inorganic fillers is important to maintain the morphology of the membrane.

The incompatibility between the inorganic fillers and the polymer matrix is another major concern of MMM formation. This condition will create the separate phases in MMM and deteriorate the gas performance of the membrane. The poor interfacial contact between the dispersed phase and the continuous phase will lead to the formation of void volume. The formation of non-selective voids at the interface will allow the bypassing of gases, which in turn decreases the membrane selectivity (Goh *et al.*, 2011). Figure 2.5 illustrates the ideal morphology of MMM and the MMM with interface voids defect (T.-S. Chung *et al.*, 2007).

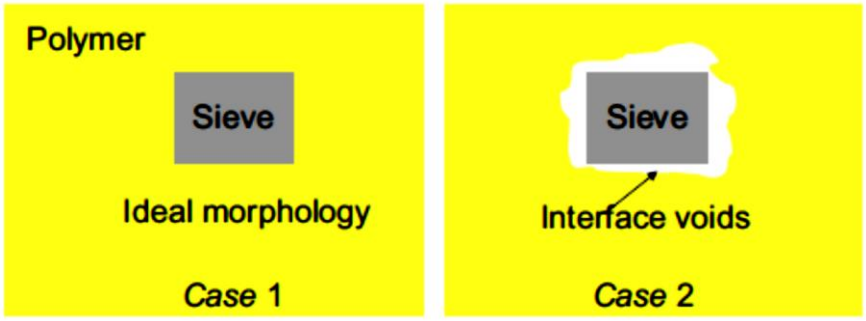

FIGURE 2.5 Schematic Diagram of Mixed Matrix Membrane Morphology

TABLE 2.3 Comparison of the Properties for Polymeric Membrane, Inorganic Membrane and MMM

Properties	Polymeric membrane	Inorganic membrane	MMM
Cost	Low	High	Moderate
Chemical and thermal stability	Moderate	High	High
Mechanical Strength	Good	Poor	Excellent
Solvent compatibility	Limited	Wide range	Limited
Swelling	Frequently occur	Free of swelling	Free of swelling
Separation performance	Moderate	Moderate	Exceeds Robeson upper boundary
Handling	Robust	Brittle	Robust

2.5 Material Selection

2.5.1 AMH-3

AMH-3 is a 3-dimensional microporous layered material with eight membered ring (8 MR) pores, built of silicate layers and interlayered spaces occupied by strontium cation, sodium cation and water molecules. The silicate layers contain plurality of tetrahedral SiO_4 units and channels extending from a top side of the one layer to a bottom side of the layer. The channels are formed from the eight membered rings (rings of eight ≡Si-O-Si≡ units) and contributes to the porosity of the material. A plurality of cations including sodium ions and strontium ions are located between the layers (Tsapatsis *et al.*, 2005). The structure of the AMH-3 layered silicate is shown in Figure 2.6 (Jeong *et al.*, 2003).

The layered silicate was first synthesized and characterized in year 2003. The formula for unit cell of AMH-3 is $Na_8Sr_8Si_{32}O_{76} \cdot 16H_2O$. In addition to its good thermal and acid stability, its crystallographic pore size of 3.4 Å is particularly useful for gas separations such as CO_2/CH_4 and H_2/N_2 (Jeong *et al.*, 2003). Table 2.4 lists the kinetic diameters of several gases (Poling *et al.*, 2001).

TABLE 2.4 Kinetic Diameters (in Ångstrom) of Various Gases

Gas	**He**	**H_2**	**CO_2**	**O_2**	**N_2**	**CH_4**
Kinetic Diameter (Å)	2.6	2.89	3.3	3.46	3.64	3.8

Choi, Coronas, Lai*, et al.* (2008) reported the fabrication of MMM by dispersing AMH-3 into polybenzimidazole (PBI) matrix. The membrane showed a twofold enhancement of selectivity for H_2/CO_2 separation. On the other hand, W.-g. Kim *et al.* (2013) delaminated swollen AMH-3 into flakes and incorporated it into cellulose acetate matrix. Enhancement in the CO_2 permeability and CO_2/CH_4 gas separation performance were observed.

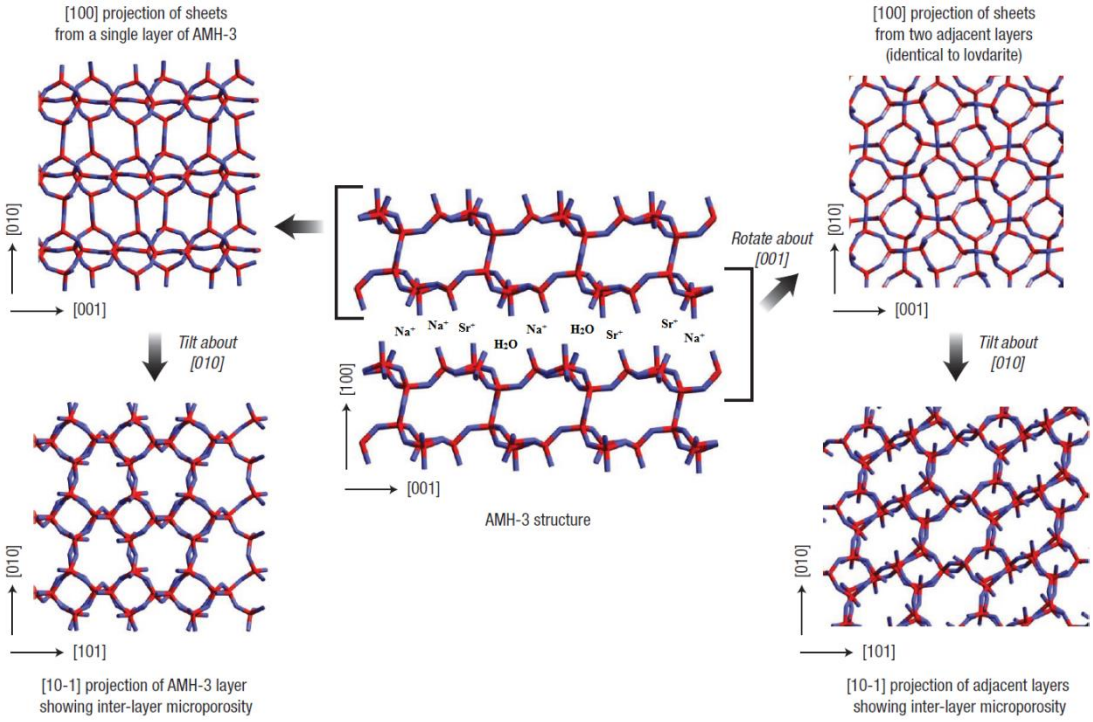

FIGURE 2.6 Structure Model of AMH-3

2.5.2 Polysulfone

Polysulfone (PSf) are an important class of engineering thermoplastics. The polymer backbone consists of para-linked aromatic groups connected by ether and sulfone and in some cases alkyl groups (Elvers *et al.*, 2003). The structure of a PSf is shown in Figure 2.7. PSf is one of the most widely studied polymeric membrane materials for CO_2/CH_4 separation.

Referring to Table 2.1, polysulfone shows the highest CO_2 permeability with good selectivity. Polysulfone is an ideal polymer phase for mixed matrix membrane as it exhibits good mechanic strength, resistance and chemical stability and cost effective (Hachisuka & Ikeda, 1999). PSf are highly resistant to hydrolysis and stable in dilute acid. The polar groups in the PSf chain contribute to the high flexural modulus while the excellent thermal stability is due to strong bonds in the backbone (Elvers *et al.*, 2003). Besides that, PSf also exhibits high resistance to plasticization at a pressure about 30 bars. Table 2.5 shows the physical properties of polysulfone (Harper, 2000).

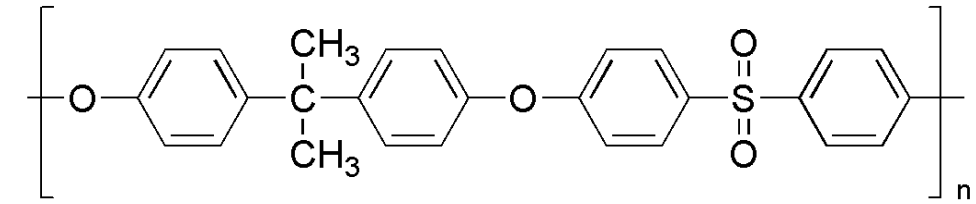

FIGURE 2.7 Structure of a Single Unit Polysulfone

TABLE 2.5 Physical Properties of Polysulfone

Properties	Value
Density (g/mL) at 25°C	1.24
Elastic Modulus (MPa)	2691
Flexural Modulus (MPa)	2553
Tensile Strength (MPa)	79
Glass Transition Temperature (°C)	190

2.6 Structural Modification of Inorganic Filler

Although the layered silicate materials showed excellent properties for MMMs, they are usually hydrophilic which results in poor interfacial interactions with non-polar polymers (Rezakazemi *et al.*, 2014). Therefore, the layered silicate materials should be made compatible with the polymer phase by surface modifications to enhance the miscibility of the layered silicate with the polymer before embedding.

Takahashi and Kuroda (2011) introduced a different covalent modification methods for the layered silicates. The modification can be carried out with different silylation reagents such as amino, thiol, and alkyl groups. The most popular type of modifier agent are silane coupling agents which have hydrolysable and organofunctional ends.

Structural modification such as swelling is necessary to enhance the interlayer spacing. However, the properties of silanol groups on AMH-3 surface and charge-balancing cations in the interlayer spaces rendered the conventional procedures for clay swelling ineffective (W.-g. Kim *et al.*, 2013). Subsequently, Choi, Coronas, Sheffel*, et al.* (2008) introduced the AMH-3 swelling process by means of proton exchange in the amino acid followed by sequential intercalation of primary amine molecules.

Furthermore, 'priming' technique is suggested to be able to improve the compatibility of the inorganic filler with the polymer (Koros *et al.*, 2003). Priming requires adding of a small amount of the total polymer required to form a membrane (typically 5–10 wt.-%) to a suspension of inorganic particles in a proper solvent. Priming of inorganic particles before dispersing in the bulk polymer can reduce stress at the interface between polymer and inorganic particles. This technique minimizes the agglomeration of inorganic particles and promotes interaction between the bulk polymer and polymer primed inorganic particles which subsequently minimizes defective interfaces (Hillock *et al.*, 2008).

CHAPTER 3

METHODOLOGY

3.1 Flow Chart of Project Activities

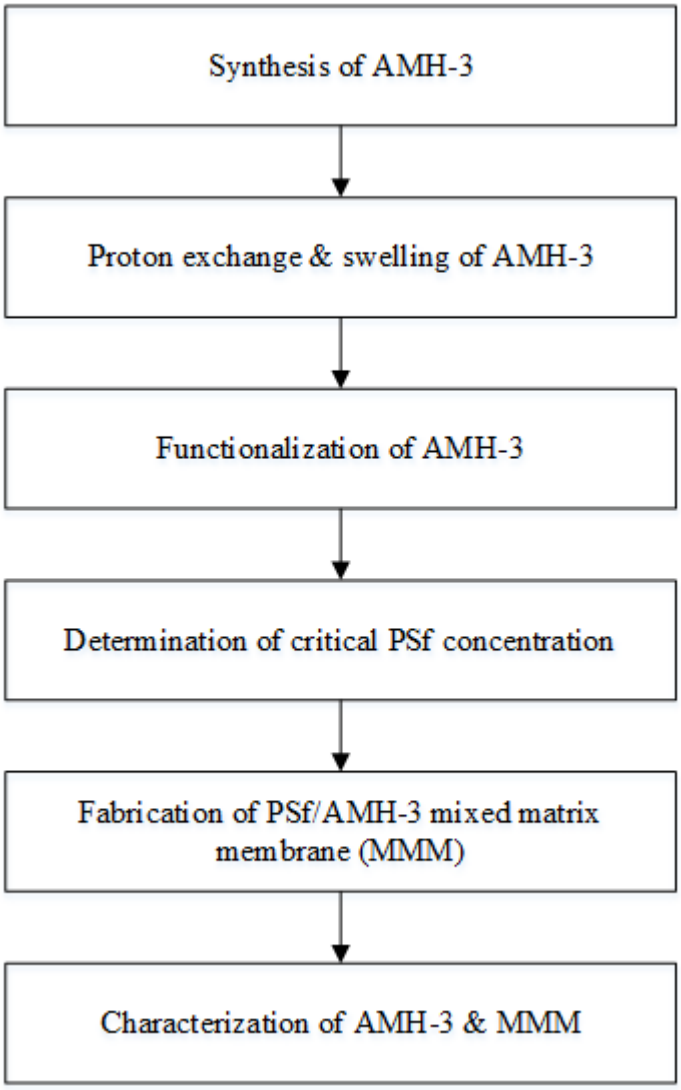

FIGURE 3.1 Flowchart of Overall Project Activities

3.2 Materials and Equipment

3.2.1 Materials

The chemicals and materials used are as follow:

- Sodium hydroxide pellets (NaOH, ≥ 99% purity, Merck)
- Strontium chloride hexahydrate ($SrCl_2 \cdot 6H_2O$, ≥ 99% purity, Sigma-Aldrich)
- Sodium silicate (≥ 99% purity, Sigma-Aldrich)
- Titanium (III) chloride ($TiCl_3$, 20% w/w solution in 2N HCl, Acros Organics)
- Polysulfone pellets (MW~35000, Sigma-Aldrich)
- N-Methyl-2-pyrrolidinone (C_5H_9NO, ≥ 99% purity, Merck)
- DL-histidine ($C_6H_9N_3O_2$, ≥ 99% purity, Sigma-Aldrich)
- Hydrochloric acid (HCl, fuming 37%, Merck)
- Dodecylamine ($C_{12}H_{27}N$, ≥ 98% purity, Sigma-Aldrich)
- Toluene ($C_6H_5CH_3$, ≥ 99.9% purity, Merck)
- Octyl(methyl)dimethoxysilane ($C_{11}H_{26}O_2Si$, ≥ 95.0% purity, Sigma-Aldrich)

3.2.2 Equipment

TABLE 3.1 List of Equipment

Equipment	Function
Magnetic hotplate stirrer	To heat and stir the solution
Teflon-lined autoclave	For hydrothermal synthesis of AMH-3
Vacuum oven	To dry the solid chemicals
Ultrasonic cleaner	To degas the dope solution and washing of AMH-3 solids
pH meter	To measure the pH of the solution
Centrifuge	To purify the swollen AMH-3
Electronic balance	To measure the weighs of the necessary chemicals
Rotational viscometer *Model: Fungilab Alpha L*	To measure the viscosity of PSf dope solutions

3.3 Experimental Procedure

3.3.1 Synthesis of AMH-3

1. 0.704g of sodium hydroxide pellets are dissolved in 28.24g of deionized water.
2. After 30 minutes of stirring, 1.502g strontium chloride hexahydrate is added into the solution while heating the solution at 80°C.
3. After 30 minutes of stirring, 6.26g sodium silicate is added drop wise to produce a white, cloudy solution.
4. After another 30 minutes of stirring, 2.17g titanium (III) chloride solution is added drop wise to obtain a dark purple, cloudy solution.
5. The solution is stirred vigorously for 60 minutes.
6. The solution is then poured into a Teflon-lined stainless steel autoclave.
7. The hydrothermal synthesis is carried out for 3 days at 200°C.
8. Crystalline AMH-3 is obtained along with colloidal amorphous material.

3.3.2 Purification of AMH-3

1. The content of the autoclave is diluted to 200ml with deionized water and kept for 1 hour in an ultrasonic bath.
2. The suspension is then decanted and the sediment is washed again with 200ml of deionized water. After 5 minutes, new sediment is obtained.
3. The washing is repeated 5 times and the precipitate is filtered.
4. The AMH-3 solids are dried overnight at 80°C in vacuum oven to obtain pure AMH-3 crystals.

3.3.3 Proton Exchange & Swelling of AMH-3

1. 0.776g of DL-histidine is dissolved in 25ml of deionized water at 60°C under vigorous stirring until a clear solution is obtained.
2. The solution is cooled down to room temperature with continuous stirring.
3. A few drops of concentrated hydrochloric acid are added until the pH of the solution is adjusted to pH 6.0.
4. 0.2g of as-made AMH-3 is added to the buffer solution and stirred vigorously to allow proton exchange.
5. The swelling agent solution is prepared by dissolving 2.061g of dodecylamine in 50ml of deionized water at 60°C and continuously stirred for 30 minutes.
6. After 1 hour from the start of proton exchange, the swelling agent solution is added drop wise.
7. After 12 hours of stirring at 60°C, the swollen AMH-3 is obtained.
8. The product is purified by washing with deionized water and centrifugation for 3 times.
9. The product is then air dried at room temperature for two days.

3.3.4 Functionalization of AMH-3

1. 0.2g of swollen AMH-3 is dried overnight in a vacuum oven at 80°C.
2. The swollen AMH-3 is added to a mixture of 4g anhydrous toluene and 0.4g of octyl(methyl)oxysilane.
3. The functionalization reaction is then carried out under reflux condition for 16 hours.
4. Pure toluene is added into the reaction vessel and agitated to wash the product.
5. The upper solvent of the suspension is decanted after the sedimentation of AMH-3 particles.
6. The washing is repeated for 3 times.
7. The product is then dried overnight at 60°C in an oven.

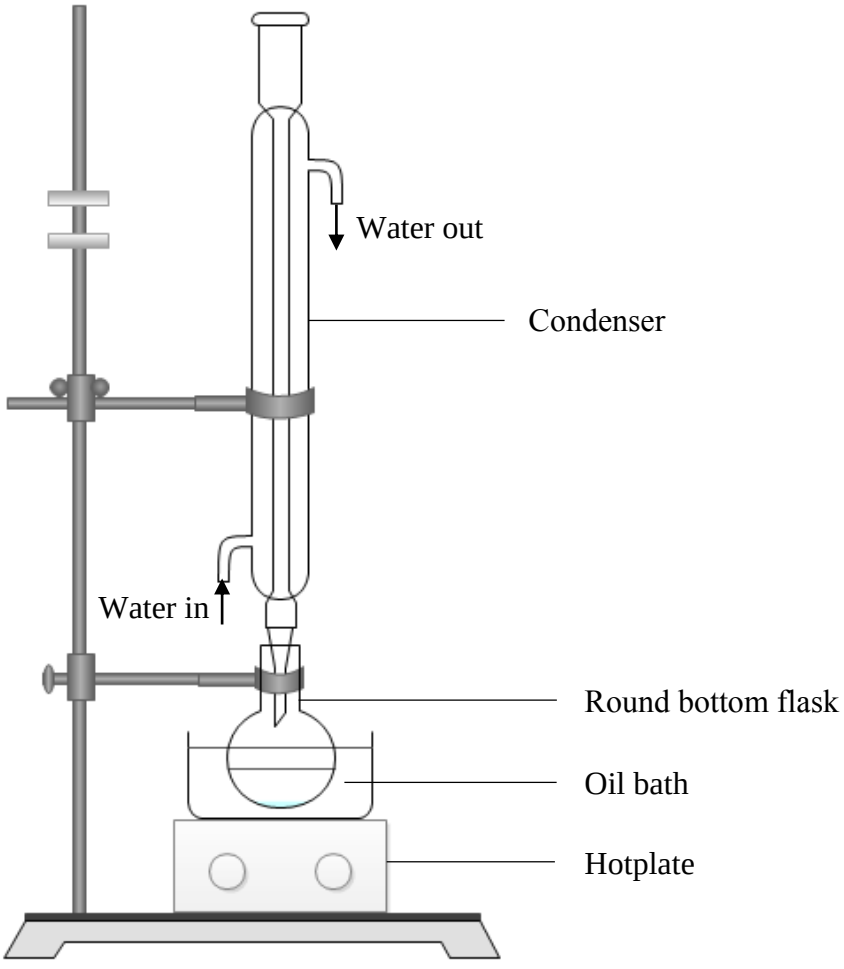

FIGURE 3.2 Experimental Setup for Functionalization of AMH-3 at Reflux Condition

3.3.5 Determination of Critical Polymer Concentration

1. PSf pellets are dried at 60-80 ºC in a drying oven for 24 hours to remove moisture.
2. 10, 15, 20, 25, 28 wt.-% PSf and corresponding wt.-% NMP solvent are used.
3. The NMP solvents are stirred on a hot plate at a temperature of 50 ºC.
4. The dried PSf pellets are slowly added into NMP while stirring.
5. Heating is stopped after all the PSf are added into the solutions. The mixtures are leaved to continuous stirring for 20 hours.
6. The viscosity of each PSf/NMP solutions are determined using the Fungilab Rotational Viscometer (Model Alpha L) at 30 rpm.
7. The readings are taken and the viscosity curve is plotted based on the readings.
8. Extrapolated lines are plotted to obtain the critical polymer concentration of PSf/NMP.

3.3.6 Fabrication of Polysulfone (PSf) Polymeric Membrane

1. PSf pellets are dried at 60-80 ºC in a drying oven for 24 hours to remove moisture.
2. 23 wt.-% PSf and 77 wt.-% NMP solvent are used.
3. NMP solvent is stirred on a hot plate at a temperature of 50 ºC.
4. The dried PSf pellets are slowly added into NMP while stirring.
5. Heating is stopped after all the PSf are added into the solution. The mixture is leaved to continuous stirring for 24 hours.
6. The dope solution is then transferred to a centrifugal tube and sealed with parafilm for degassing purpose.
7. Degassing is carried out for 4 hours to remove the gas bubbles in the dope solution.
8. After degassing is done, the dope solution is left for standing in the lab at room temperature for 24 hours.
9. The dope solution is again put for degassing for 30 minutes and leave for standing 30 minutes to fully remove additional gas bubbles if necessary.
10. A clean glass plate is washed with acetone and dried completely using compressed air.
11. The dope solution is now ready to be casted. The homogenous mixture is poured onto the glass plate.
12. Membrane casting is then performed with the casting knife and film thickness is 200 μm.
13. The casting knife is pulled from upper to lower of the glass plate to form the membrane film. Speed should be consistent to prevent defects.
14. After casting, the film is left to evaporate for 60 seconds on the glass plate.
15. The glass plate with the film is immersed into coagulation bath which is half filled up with distilled water for 24 hours.
16. Membrane is finally dried at room temperature for another 48 hours.

3.3.7 Fabrication of PSf/AMH-3 MMM

1. 1 wt.-% / 3 wt.-% / 5 wt.-% of AMH-3 is dissolved in NMP solvent.
2. The solution is put into an ultrasonic bath for 30 minutes to break the aggregates of AMH-3.
3. 10% of the required PSf is added into the solution and stirred for 6 hours.
4. The remaining of the PSf pellets is added into the solution and stirred for 12 hours.
5. The solution is sonicated for 30 minutes to remove bubbles.
6. The solution is poured on a glass plate and casted using casting knife.
7. After casting, the film is left to evaporate for 60 seconds on the glass plate.
8. The glass plate with the film is immersed into coagulation bath which is half filled up with distilled water for 24 hours.
9. Membrane is finally dried at room temperature for another 48 hours.

3.3.8 Characterization of AMH-3 and MMM

TABLE 3.2 Characterization Techniques

Technique	Description
Fourier Transform Infrared Spectrometer (FT-IR) *Model: Perkin Elmer Spectrum One*	**Purpose:** To determine the functional groups and the silane modified grafting in the AMH-3 layered silicate. **Procedure:** Samples are pulverized and pelletized with KBr. Range of wavelength: 4000-2500 cm^{-1} and 1300-400 cm^{-1}
X-Ray Diffraction (XRD) *Model: Bruker AXS D8 Advance*	**Purpose:** To study the crystallographic structure of AMH-3. **Parameters:** Cu Kα radiation in (10° – 40°) 2θ range, step size 2θ = 0.02
Surface Area Analyzer and Porosimetry System (SAP) *Model: Micromeritics ASAP 2020*	**Purpose:** To determine the surface area and pore size of the AMH-3. **Procedure**: Samples are degassed overnight. Nitrogen adsorption isotherms were performed at −196 °C.
Scanning Electron Microscopy (SEM) *Model: Hitachi TM 3030*	**Purpose:** To study the surface and cross-section morphology of MMM. **Procedure**: Samples are freeze-fractured in liquid nitrogen, coated with platinum and viewed under operating acceleration voltage of 15 kV.
Energy Dispersive X-Ray (EDX) Spectrometry *Model: Bruker Quantax 70*	**Purpose:** To identify the presence and dispersion of inorganic filler in MMM.
Thermal Gravimetric Analysis (TGA) *Model: Perkin Elmer STA 6000*	**Purpose:** To investigate the thermal stability of MMM. **Procedure**: Samples are heated from 30°C to 800°C with N_2 purging at a heating rate of 10°C/min.
Contact Angle Analysis *Model: ramé-hart Model 290*	**Purpose:** To determine the hydrophobicity of the MMM. **Procedure**: Images of water droplets on the membrane surface were captured and the contact angle is measured using drop shape analytical system.

3.4 Gantt Chart

TABLE 3.3 Gantt Chart

No.	Project Activities	Final Year Project I													
		Week													
		1	2	3	4	5	6	7	8	9	10	11	12	13	14
1	Confirmation of project topic														
2	Preliminary research work and literature review														
3	Experimental planning														
4	Acquisition of chemicals, glassware and equipment														
5	Submission of extended proposal														
6	Viscometric test														
7	Proposal defense														
8	Submission of interim draft report												•		
9	Submission of interim report													•	
10	Synthesis of AMH-3														

- **Milestone**

No.	Project Activities	Final Year Project II													
		Week													
		1	2	3	4	5	6	7	8	9	10	11	12	13	14
1	Synthesis of AMH-3	■	■	●											
2	Modification of AMH-3	■	■	■	●										
3	Fabrication of AMH-3/PSf MMM			■	■	■	●								
4	Fabrication of modified AMH-3/PSf MMM					■	■	■	■	●					
5	Characterization of AMH-3							■	■	■	●				
6	Characterization of MMM							■	■	■	●				
7	Validation of experimental data							■	■	■	■				
8	Submission of progress report								●						
9	Pre – SEDEX											■			
10	Submission of draft final report												●		
11	Submission of dissertation (soft bound)													●	
12	Submission of technical paper													●	
13	Viva														■
14	Submission of dissertation (hard bound)														●

CHAPTER 4

RESULTS AND DISCUSSION

4.1 Determination of Critical Polymer Concentration

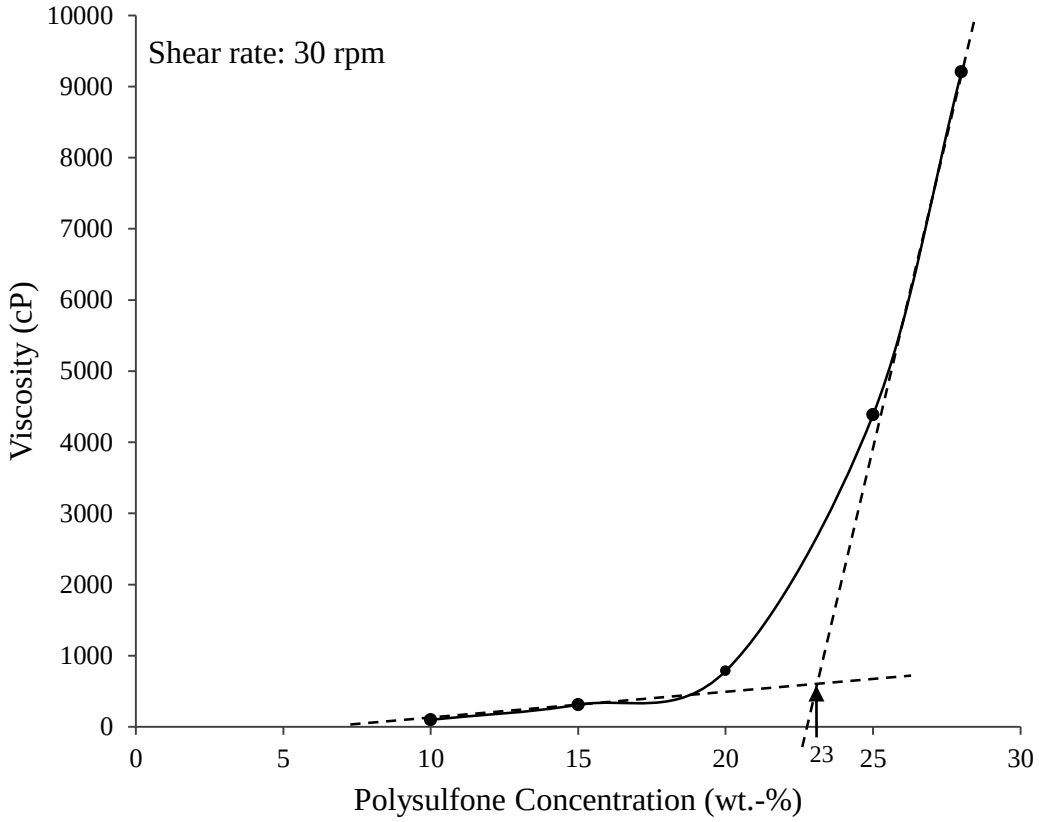

FIGURE 4.1 Viscosity vs. Polymer Concentration for PSf/NMP Dope Solutions

The viscosity curve of PSf/NMP is shown in Figure 4.1. A sharp slope is observed as the PSf concentration increases above 20 wt.-%. According to T. S. Chung *et al.* (1997), the critical concentration for a polymer/solvent binary system can be determined by the intersection of extrapolation lines of the two linear parts of the viscosity curve. Based on Figure 4.1, the critical concentration of PSf/NMP dope solution is determined to be 23 wt.-%.

Referring to Peng *et al.* (2008), the critical polymer concentration obtained for PSf/NMP was 29 wt.-%. However, the critical concentration obtained from this experiment is 23 wt.-%. This is most likely due to the difference in molecular weight of the PSf used. The polysulfone pellets used by Na Peng et al is Udel P-3500 which has an average molecular weight 78000 g/mol with polydispersity index of 3.51, while the average molecular weight of PSf pellets used in this project is only around 35000 g/mol with polydispersity index of 2.19. Yeo *et al.* (2002) proposed that the critical polymer concentration increases with the increase of the average molecular weight and polydispersity of the polymer. Therefore, the result obtained is justified as the average molecular weight and polydispersity of the PSf used are lower compared to Peng *et al.* (2008).

The critical concentration exists due to the intimate intermolecular interactions and significant polymer chain entanglements (Peng *et al.*, 2008). Chain entanglement, a nonpermanent structural interaction among polymer chains occurs at high polymer concentration and the entanglement releases gradually as the solvent concentration increases (Bird *et al.*, 1987; Lin, 2003). Below the critical concentration, polymer chains are loosely packed and have high degree of freedom. As a result, the nonsolvent tend to diffuse and penetrate into the chain spaces of polymer solution and subsequently form macrovoids. When the polymer concentration exceeds the critical value, the polymer chains form entanglements as they become closely packed, which makes the polymer to be more solid-like. Such entangled network structure makes membranes stronger to balance shrinkage stress, hinders the nonsolvent intrusion, and hence suppress defects such as the macrovoids formation (Peng *et al.*, 2008).

Thereafter, all the mixed matrix membranes are casted using 23 wt.-% PSf while varying only the AMH-3 loadings.

4.2 Characterization Results of Pristine and Functionalized AMH-3

4.2.1 Fourier Transform Infrared (FT-IR) Analysis

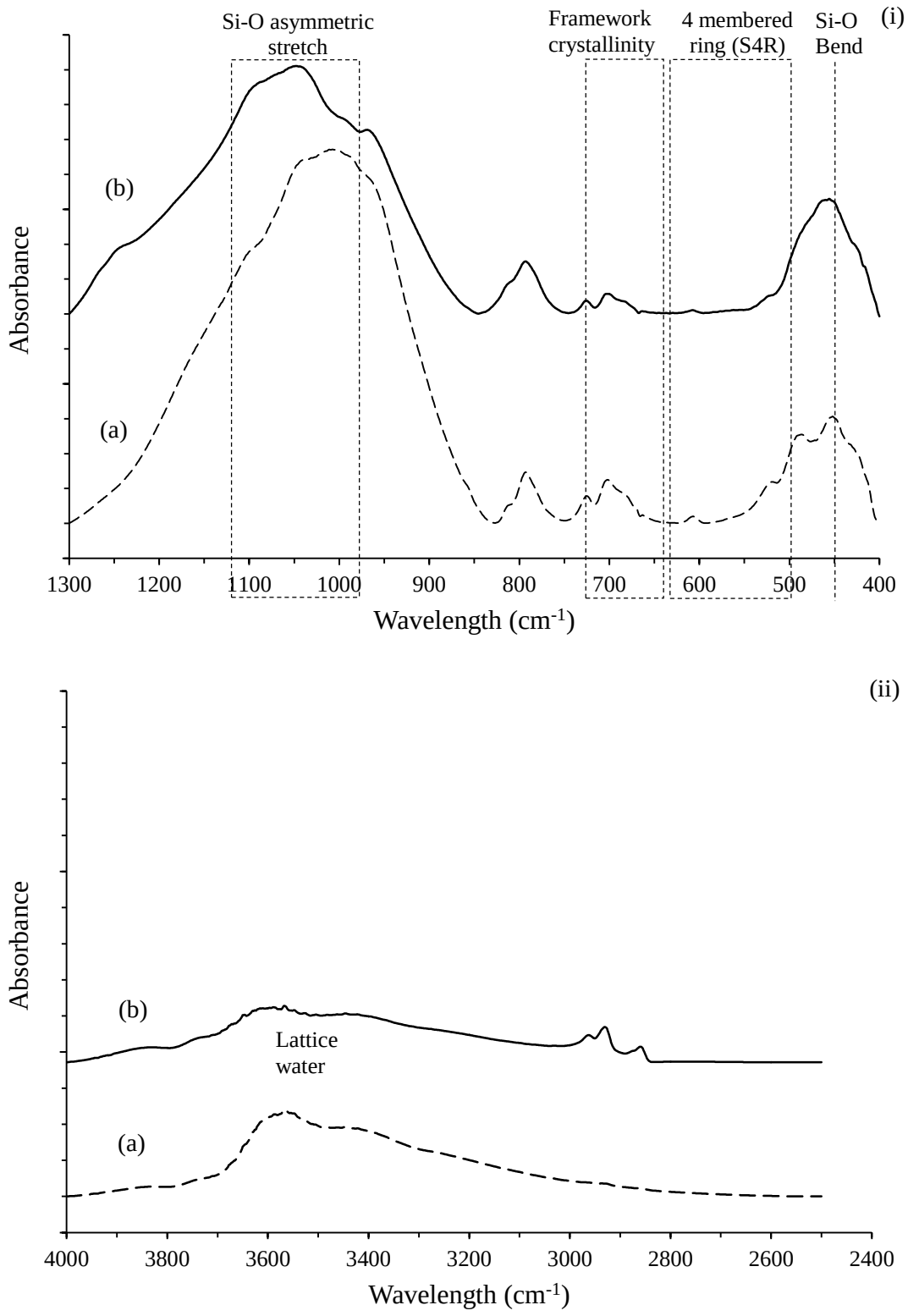

FIGURE 4.2 FT-IR Spectra of (a) Pristine AMH-3 and (b) Functionalized AMH-3 at Wavelength of (i) 1300 to 400 cm^{-1} and (ii) 4000 and 2500 cm^{-1}.

Figure 4.2 shows the FT-IR spectra of the pristine and functionalized AMH-3. Vibrational bands of nanoporous oxide materials measured between 1300 and 400 cm^{-1} represent the internal Si-O linkages of the SiO_4 tetrahedral as well as the external linkages interacting with other tetrahedral or chemical species (Nair *et al.*, 2005). On the other hand, the spectra in the range of 4000 to 2500 cm^{-1} provide information on the interlayer hydroxyls and can be used to identify different types of silanol protons (Morrow & Gay, 2000).

Layer structure of pristine AMH-3 is built of single four-membered rings (S4R) including four silicon atoms (Si1, Si2, Si3, and Si4) (Jeong *et al.*, 2003). The S4Rs are assigned to the bands between 650 and 500 cm^{-1}, while the bands between 1150 and 1050 cm^{-1} are ascribed to the external linkages of Si-O asymmetric stretch (Nair *et al.*, 2005). Bands shown around 3600 cm^{-1} can be attributed to the hydroxyl stretching frequencies of the lattice water which is situated in the interlayer space of original framework (Jeong *et al.*, 2003). The FT-IR spectra for pristine AMH-3 corresponds to the band assignments obtained from literature, indicating the successful synthesis of AMH-3 layered silicate.

Structural changes can be observed in FT-IR spectra after the functionalization of AMH-3 layered silicate. The absorption bands between 500 and 420 cm^{-1} corresponding to Si-O bend are replaced by only a single band after functionalization. The absorption bands between 650 and 500 cm^{-1} corresponding to S4Rs become insignificant after functionalization.

Furthermore, functionalized AMH-3 shows absorption bands of lower intensity in the range of 720 and 650 cm^{-1}. As the intensity of these bands are pertained to the crystallinity of frameworks, thus the decrease in signal intensities indicates that the crystallinity decreases (Lezcano *et al.*, 1997).

The pristine and functionalized AMH-3 show considerable differences in the bands between 4000 and 2500 cm^{-1}. The absorption band around 3600 cm^{-1} for lattice water is no longer noticeable after the functionalization of AMH-3 as it is being replaced by the swelling or functionalization agent. Also, the functionalized AMH-3 shows absorption bands between 3000 and 2850 cm^{-1}, similar to swollen AMH-3 which are suggested to be the C–H stretching of $–CH_2–$ aliphatic chains and CH_3. The

FT-IR spectra of functionalized AMH-3 showed good agreement with the spectra of swollen AMH-3 in the paper by Choi, Coronas, Sheffel*, et al.* (2008).

4.2.2 X-Ray Diffraction (XRD) Analysis

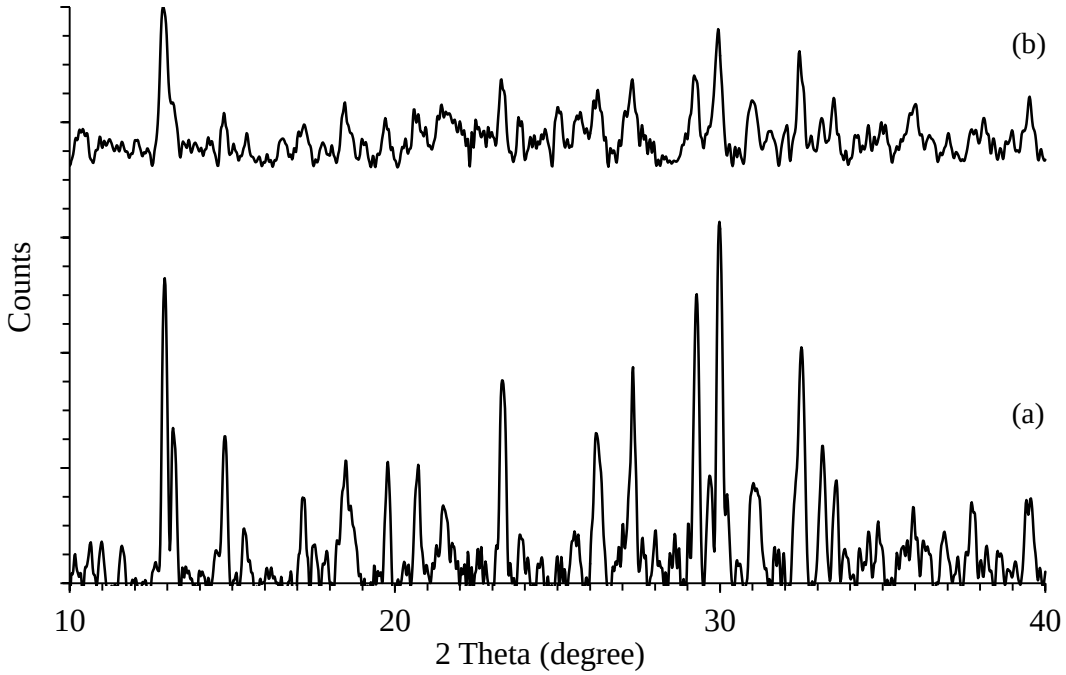

FIGURE 4.3 XRD Pattern of (a) Pristine AMH-3 (b) Functionalized AMH-3

Figure 4.3 shows the XRD patterns of as-synthesized AMH-3 and functionalized AMH-3. The characteristic peaks of as-synthesized AMH-3 in FIGURE 4.3a indicate the crystalline structure of AMH-3 layered silicate, which is in good agreement with the previous study by Choi, Coronas, Sheffel*, et al.* (2008).

According to Choi, Coronas, Sheffel*, et al.* (2008), the AMH-3 layered silicate becomes amorphous after the proton exchange step. Furthermore, the amorphous structure of the proton-exchanged AMH-3 is maintained throughout the swelling and functionalization steps (W.-g. Kim *et al.*, 2011). Consistent with the FT-IR results, the XRD pattern of functionalized AMH-3 in Figure 4.3b illustrates the decrease in crystallinity as it becomes amorphous in structure.

4.2.3 Surface Area and Pore Size (SAP) Analysis

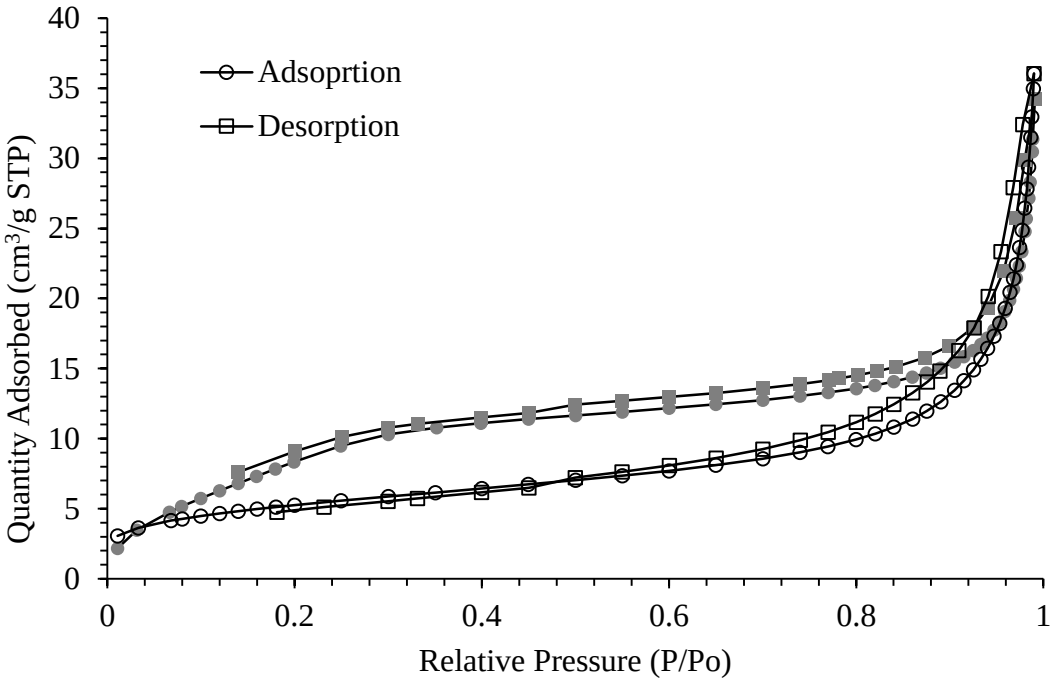

FIGURE 4.4 N_2 Physisorption Isotherms for Pristine and Functionalized AMH-3

Figure 4.4 shows the N_2 physisorption isotherms for pristine and functionalized AMH-3. With respect to IUPAC classification of adsorption isotherm, the pristine AMH-3 exhibits an adsorption behavior corresponding to type III, whereas the isotherm of the functionalized AMH-3 is associated to type II. Both materials of type II and type III isotherms are categorized as macroporous (Sing *et al.*, 1985). The low porosity of the material is possibly due to the small size of 8 MR apertures and the blocking of pore by intra and interlayer cations (Choi, Coronas, Sheffel*, et al.*, 2008).

The specific surface areas are determined using the Brunauer–Emmett–Teller (BET) technique and the pore size averages are calculated using the Barrett–Joyner–Halenda (BJH) method. The specific surface area of pristine AMH-3 is obtained to be 18.75 m^2/g and the pore size is 145.27 Å. The functionalized AMH-3 showed a BET surface area of 37.16 m^2/g and pore size of 63.35 Å.

The increase in surface area after functionalization is most likely due to the attachment of alkoxysilane to the layer of the inorganic filler (W.-g. Kim *et al.*, 2011). On the other hand, the decrease of pore size of functionalized AMH-3 might be resulted by the pore space of the layered silicate being occupied by the bonded alkyl phase (Jal *et al.*, 2004).

4.3 Characterization Results of Mixed Matrix Membranes

4.3.1 Scanning Electron Microscopy (SEM) Analysis

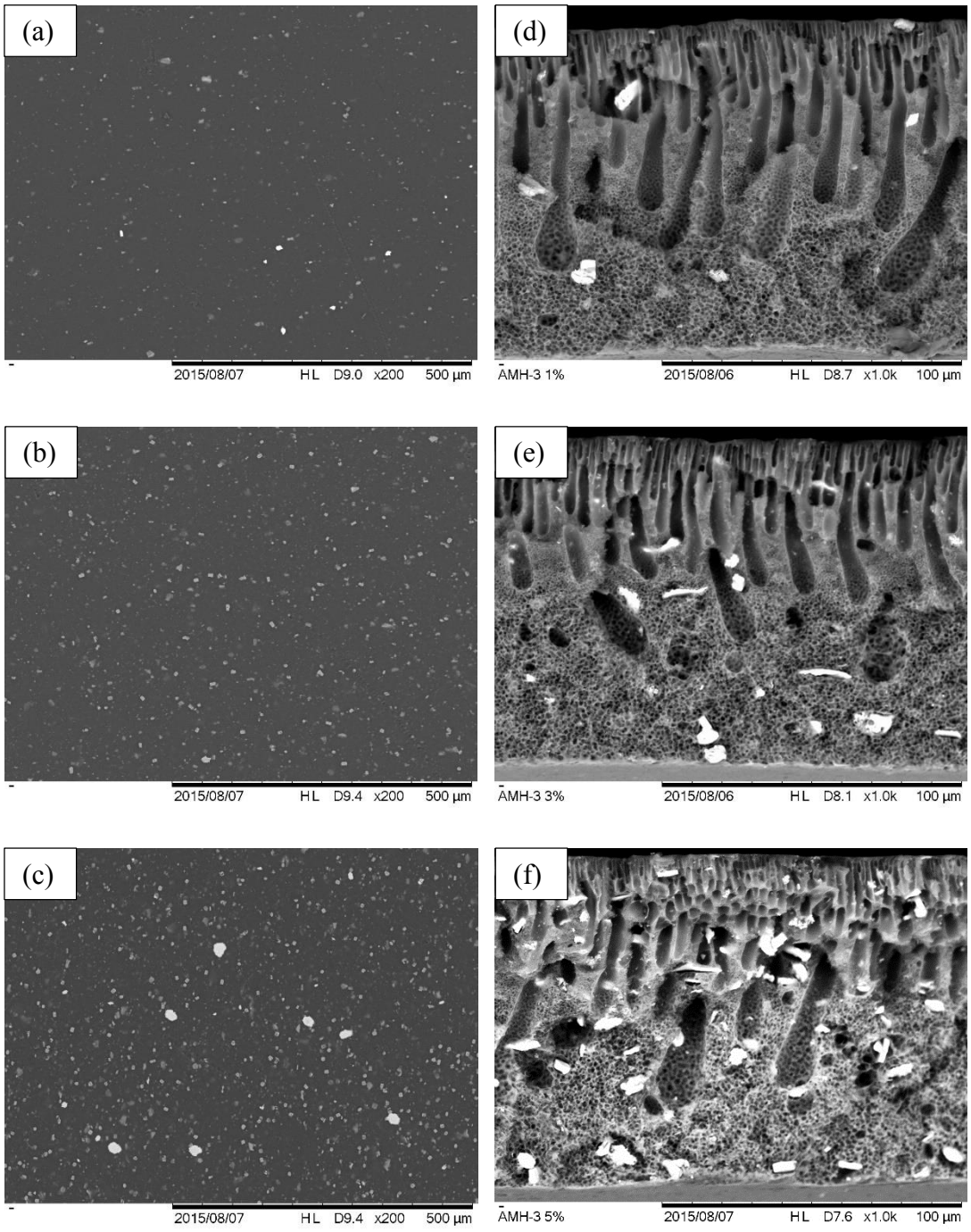

FIGURE 4.5 Surface Morphology for MMM with Different Loadings of AMH-3 at (a) 1 wt.-%, (b) 3 wt.-%, and (c) 5 wt.-%; and Cross-Section Morphology of MMM with (d) 1 wt.-%, (e) 3 wt.-%, and (f) 5 wt.-% of AMH-3.

SEM characterization is aimed to determine the extent of adhesion and dispersion of AMH-3 in PSf matrix. Figure 4.5 illustrates the surface and cross-sectional morphologies of MMM with different loadings of pristine AMH-3. Particle distribution in matrix continuous phase is an important factor that affects the performance of MMM (Aroon *et al.*, 2010). The uniform scattering of white particles on the surface of MMM implies good distribution and dispersion of AMH-3 in Figure 4.5a, 4.5b and 4.5c. The particles tend to agglomerate as the filler loading increases, due to the increase contact of the particles. At 5 wt.-% of AMH-3 loading in MMM, big white spots of the filler are observed on the surface morphology, indicating particle agglomeration. Therefore, the optimum loading of the pristine AMH-3 in MMM is most likely 3 wt.-%.

Figure 4.5d, 4.5e and 4.5f show the cross-sectional images of MMM at increasing loading of AMH-3. All of the MMMs show finger-like voids. It is observed that there are minimal formation of voids surrounding the AMH-3 fillers.

Figure 4.6 shows the surface and cross-sectional images of MMM incorporated with functionalized AMH-3. Similar to MMM of pristine AMH-3, the surface morphologies of MMM with functionalized AMH-3 show good distribution and dispersion of AMH-3 fillers. No obvious particle agglomeration of functionalized AMH-3 is observed in the surface morphology of MMMs.

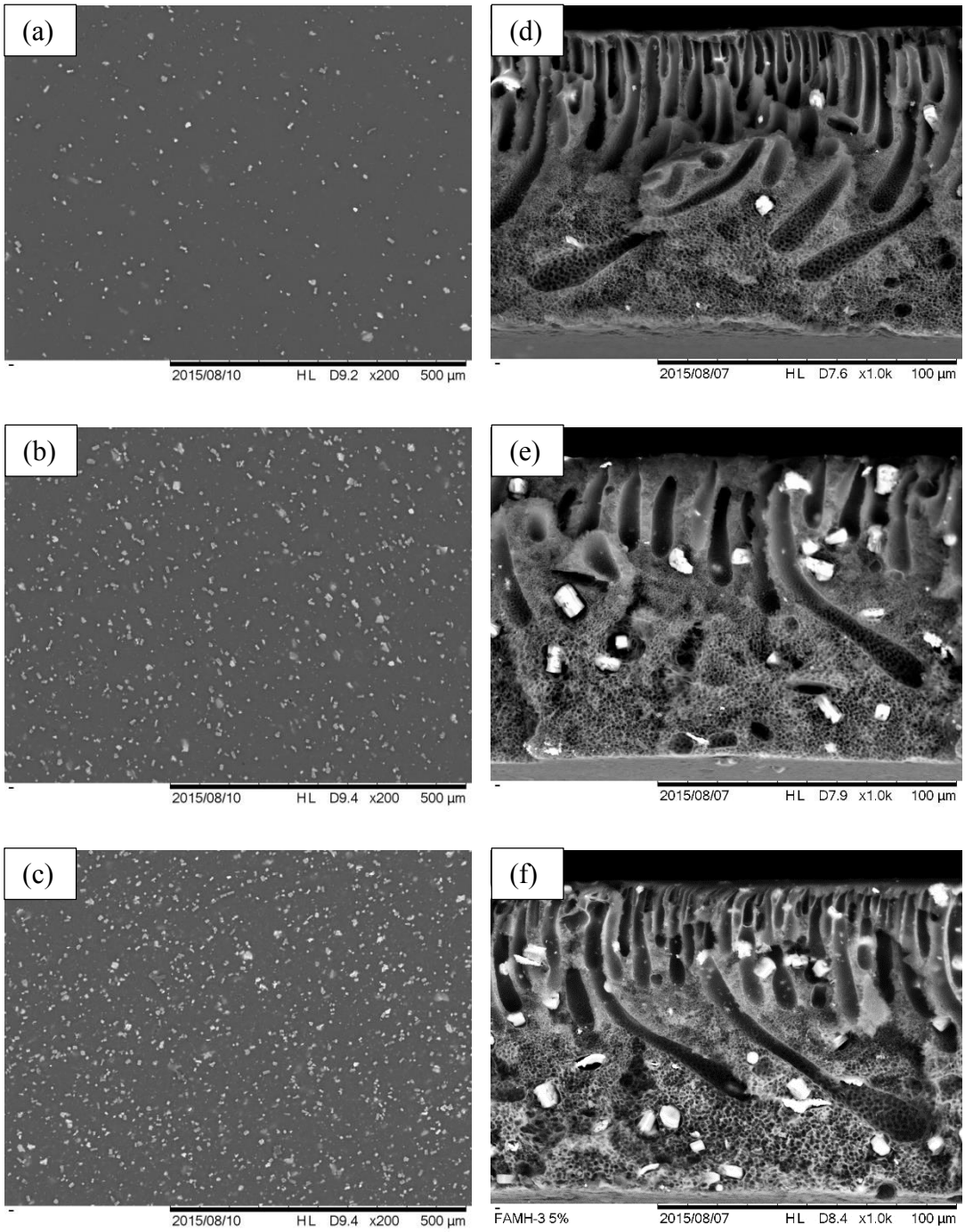

FIGURE 4.6 Surface Morphology for MMM with Different Loadings of Functionalized AMH-3 at (a) 1 wt.-%, (b) 3 wt.-%, and (c) 5 wt.-%; and Cross-Section Morphology for MMM with (d) 1 wt.-%, (e) 3 wt.-%, and (f) 5 wt.-% of Functionalized AMH-3.

4.3.2 Energy Dispersive X-ray (EDX) Analysis

TABLE 4.1 Elemental Composition of MMM Incorporated with Pristine AMH-3

PSf/AMH-3	**1wt.-%**	**3wt.-%**	**5wt.-%**
Element	Weight %		
C	73.26	69.73	65.90
O	19.18	21.39	24.43
S	6.78	6.34	5.33
Si	0.77	2.54	4.34

TABLE 4.2 Elemental Composition of MMM Incorporated with Functionalized AMH-3

PSf/FAMH-3	**1wt.-%**	**3wt.-%**	**5wt.-%**
Element	Weight %		
C	71.79	69.09	67.13
O	21.01	22.56	22.89
S	6.44	5.42	5.48
Si	0.76	2.93	4.50

The composition of the major elements in the MMM incorporated with pristine AMH-3 and functionalized AMH-3 are listed in Table 4.1 and Table 4.2. The silicon content verifies the presence of AMH-3 in the MMM, whereas the sulfur element indicates the PSf polymer. Based on the EDX analysis, the weight percent of silicon element is consistent with the loading amount of AMH-3 in MMM.

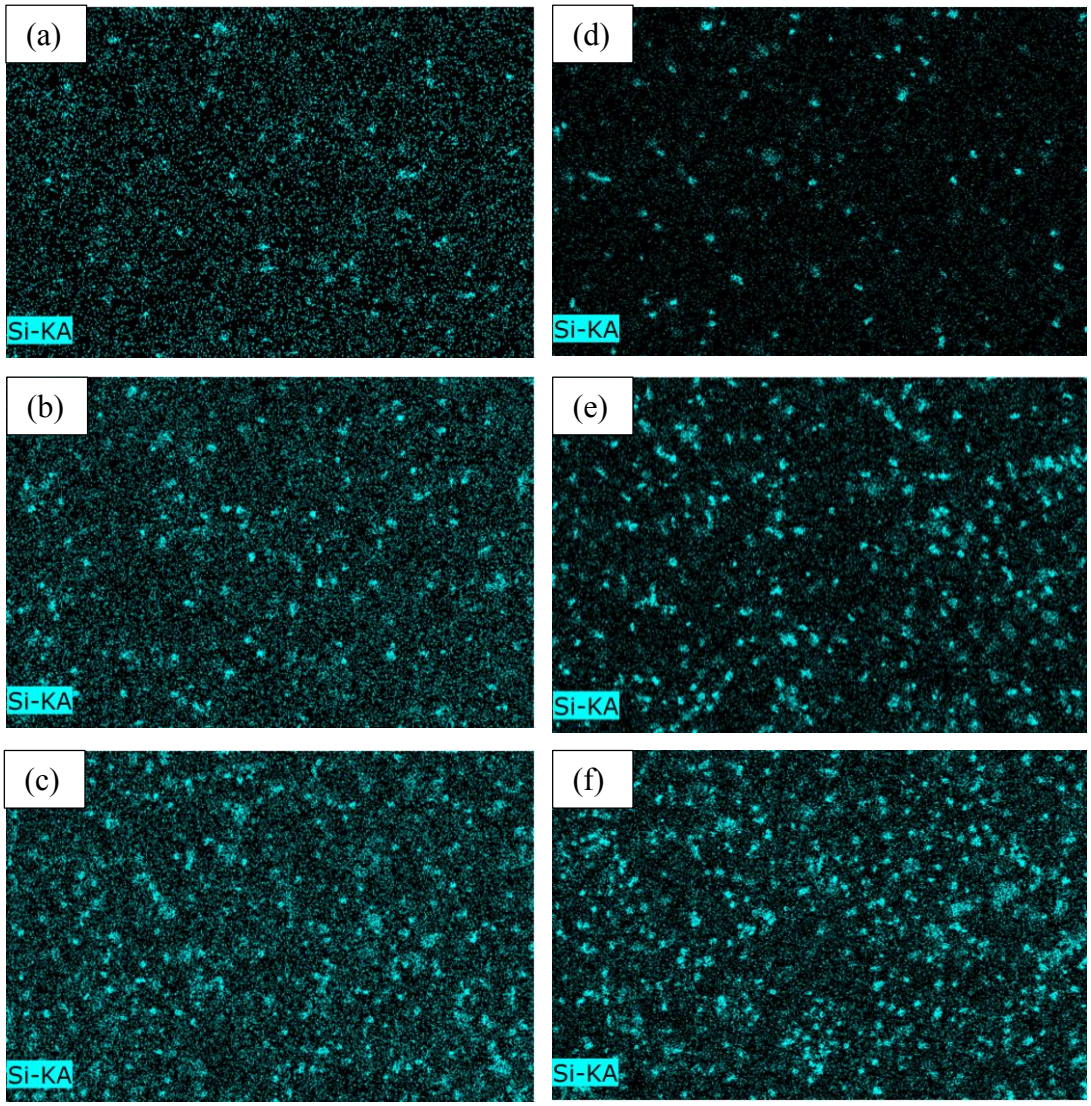

FIGURE 4.7 Element Mapping of Silicon for MMM Incorporated with Pristine AMH-3 of (a) 1 wt.-%, (b) 3 wt.-%, (c) 5 wt.-% and (e) 1 wt.-%, (f) 3 wt.-%, (g) 5 wt.-% of Functionalized AMH-3.

Figure 4.7 illustrates the mapping of silicon in MMM for different loading of pristine and functionalized AMH-3. In agreement with the SEM analysis, the uniform scattering of silicon element indicates good distribution and dispersion of the AMH-3 filler in the MMM.

In summary, the surface and cross-sectional morphologies of both pristine AMH-3 MMM and functionalized AMH-3 MMM are quite similar. The gas separation performance of MMM is highly affected by the morphologies of MMM. The MMM showing good adhesion and dispersion of both pristine and functionalized AMH-3 are expected to show good gas separation performance.

4.3.3 Contact Angle (CA) Analysis

Contact angles of the membranes were measured using contact angle goniometer at room temperature, in order to examine the surface properties of the membranes. Images of water droplets on the membrane surface were captured by a computer controlled video capture system. The contact angle for each samples are listed in Table 4.3.

TABLE 4.3 Contact Angle of Mixed Matrix Membranes

Sample	Contact Angle (°)
Pure PSf	66.6
PSf/1wt% AMH-3	64.4
PSf/3wt% AMH-3	63.7
PSf/5wt% AMH-3	62.1
PSf/1wt% FAMH-3	68.0
PSf/3wt% FAMH-3	70.8
PSf/5wt% FAMH-3	83.5

Based on Table 4.3, it is observed that mixed matrix membranes incorporated with pristine AMH-3 are more hydrophilic as the contact angle are smaller; whereas, the MMM with functionalized AMH-3 showed greater hydrophobicity with larger contact angle. This proves that the modification of AMH-3 increases its hydrophobicity. Koyano *et al.* (1997) have shown similar findings in which the MCM-48 and MCM-41 silicas became more hydrophobic after functionalization by trimethylsilylation. The increase of hydrophobicity in AMH-3 allows better compatibility with polysulfone which is hydrophobic in nature.

4.3.3 Thermal Gravimetric Analysis (TGA)

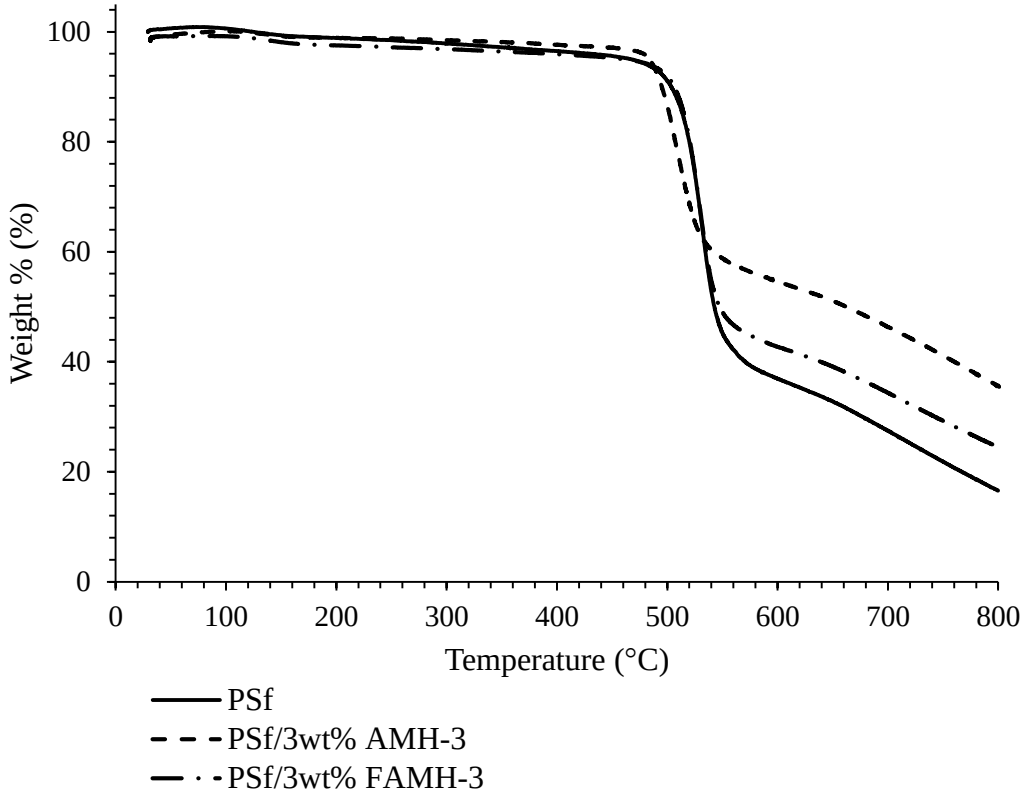

FIGURE 4.8 TGA Curves of Neat PSf Membrane and MMMs

Thermal gravimetric analyzer measures the mass loss of a polymer as a function of temperature. The samples are heated from 30°C to 800°C with a rate of 10°C/min. Figure 4.8 shows the weight loss curves of PSf membrane and MMMs.

Generally, MMMs are expected to exhibit enhanced thermal stability by incorporation of inorganic fillers. Based on Figure 4.8, the neat PSf membrane shows a substantial weight loss occurring at around 530°C.

As for MMM with pristine AMH-3, the degradation takes place at a slightly lower temperature of 510°C. This is probably due to the desorption of strongly-bounded water molecules binding in the gallery space (Choi, Coronas, Sheffel*, et al.*, 2008). The functionalized AMH-3 MMM shows a decomposition temperature at 530°C indicating slight improvement of the thermal stability of AMH-3 by functionalization.

The residual mass of MMM with pristine AMH-3 is the highest followed by the MMM with functionalized AMH-3, while the pure PSf membrane showed the lowest residual weight at 800°C.

It can be assumed that the thermal stability of PSf is not changed to great extent by the incorporation of pristine and functionalized AMH-3.

CHAPTER 5

CONCLUSION AND RECOMMENDATIONS

5.1 Conclusion

AMH-3 layered silicate was successfully synthesized via hydrothermal synthesis and subsequently verified by FT-IR and XRD analysis. Surface modification of AMH-3 was then carried out by proton exchange and swelling followed by functionalization using silane group. The functionalization of AMH-3 can be further validated by NMR analysis. After functionalization, the AMH-3 shows higher surface area and reduced pore size.

The critical concentration of PSf in NMP solvent was determined by viscometric method as 23 wt.-%. All the MMMs are casted with the optimum concentration of 23 wt.-%.

Mixed matrix membranes were then fabricated with 1, 3, 5 wt.-% of pristine and functionalized AMH-3 in polysulfone matrix. The SEM analysis shows good distribution and dispersion of AMH-3 in MMM. The surface and the cross-sectional morphology of pristine and functionalized AMH-3 are similar. The functionalization of AMH-3 is found to improve the hydrophilicity of the AMH-3 and thus allow better adhesion and compatibility with polysulfone. Based on the thermal gravimetric analysis, incorporation of AMH-3 and functionalized AMH-3 into MMM show similar TG curves.

The incorporation of pristine and functionalized AMH-3 in PSf membrane is expected to enhance the gas separation performance of the membrane.

5.2 Recommendations

The following are some recommendations for future implementation on the project:

- Improve the proton exchange, swelling and functionalization steps for AMH-3 to be more effective and efficient.
- Conduct gas permeation test for the MMMs to study the gas separation performance.
- Incorporate AMH-3 inorganic filler into different polymers such as polyimide, polyethersulfone.

REFERENCES

Abu Bakar, W. A. W., Ali, R., & Toemen, S. (2012). Catalytic methanation reaction over supported nickel–ruthenium oxide base for purification of simulated natural gas. *Scientia Iranica, 19*(3), 525-534.

Ahmad, A. L., Jawad, Z. A., Low, S. C., & Zein, S. H. S. (2012). Prospect of mixed matrix membrane towards CO2 separation. *Journal of Membrane Science & Technology*.

Ahn, J., Chung, W.-J., Pinnau, I., & Guiver, M. D. (2008). Polysulfone/silica nanoparticle mixed-matrix membranes for gas separation. *Journal of Membrane Science, 314*(1–2), 123-133.

Aroon, M. A., Ismail, A. F., Matsuura, T., & Montazer-Rahmati, M. M. (2010). Performance studies of mixed matrix membranes for gas separation: A review. *Separation and Purification Technology, 75*(3), 229-242.

Bakhtiari, O., & Sadeghi, N. (2014). The Formed Voids around the Filler Particles Impact on the Mixed Matrix Membranes' Gas Permeability. *International Journal of Chemical Engineering and Applications, 5*(2), 198-203.

Bird, R. B., Armstrong, R. C., & Hassager, O. (1987). *Dynamics of polymeric liquids. Vol. 1, 2nd Ed. : Fluid mechanics*.

Brunetti, A., Bernardo, P., Drioli, E., & Barbieri, G. (2010). Membrane Engineering: Progress and Potentialities in Gas Separations *Membrane Gas Separation* (pp. 279-312): John Wiley & Sons, Ltd.

Choi, S., Coronas, J., Lai, Z., Yust, D., Onorato, F., & Tsapatsis, M. (2008). Fabrication and gas separation properties of polybenzimidazole (PBI)/nanoporous silicates hybrid membranes. *Journal of Membrane Science, 316*(1–2), 145-152.

Choi, S., Coronas, J., Sheffel, J. A., Jordan, E., Oh, W., Nair, S., Shantz, D. F., & Tsapatsis, M. (2008). Layered silicate by proton exchange and swelling of AMH-3. *Microporous and Mesoporous Materials, 115*(1–2), 75-84.

Chung, T.-S., Jiang, L. Y., Li, Y., & Kulprathipanja, S. (2007). Mixed matrix membranes (MMMs) comprising organic polymers with dispersed inorganic fillers for gas separation. *Progress in Polymer Science, 32*(4), 483-507.

Chung, T. S., Teoh, S. K., & Hu, X. (1997). Formation of ultrathin high-performance polyethersulfone hollow-fiber membranes. *Journal of Membrane Science, 133*(2), 161-175.

Elvers, B., Hawkins, S., & Russey, W. E. (2003). *Ullmann's encyclopedia of industrial chemistry*. Weinheim; Cambridge: Wiley-VCH.

Fryxell, G. E., & Cao, G. (2012). *Environmental Applications of Nanomaterials: Synthesis, Sorbents and Sensors*: Imperial College Press.

Goh, P. S., Ismail, A. F., Sanip, S. M., Ng, B. C., & Aziz, M. (2011). Recent advances of inorganic fillers in mixed matrix membrane for gas separation. *Separation and Purification Technology, 81*(3), 243-264.

Hachisuka, H., & Ikeda, K. (1999). Polysulfone semipermeable membrane and method of manufacturing the same: Google Patents.

Harper, C. A. (2000). *Modern plastics handbook*: McGraw-Hill.

Hashemifard, S. A., Ismail, A. F., & Matsuura, T. (2011). Effects of montmorillonite nano-clay fillers on PEI mixed matrix membrane for CO2 removal. *Chemical Engineering Journal, 170*(1), 316-325.

Hillock, A. M. W., Miller, S. J., & Koros, W. J. (2008). Crosslinked mixed matrix membranes for the purification of natural gas: Effects of sieve surface modification. *Journal of Membrane Science, 314*(1–2), 193-199.

Hołda, A. K., Aernouts, B., Saeys, W., & Vankelecom, I. F. J. (2013). Study of polymer concentration and evaporation time as phase inversion parameters for polysulfone-based SRNF membranes. *Journal of Membrane Science, 442*, 196-205.

Holmes, A. S., Ryan, J. M., Price, B. C., & Styring, R. E. (1982). Process improves acid gas separation. *Journal Name: Hydrocarbon Process.; (United States); Journal Volume: 61*, Medium: X; Size: Pages: 131-136.

Ismail, A. F., & David, L. I. B. (2001). A review on the latest development of carbon membranes for gas separation. *Journal of Membrane Science, 193*(1), 1-18.

Ismail, A. F., & Lorna, W. (2002). Penetrant-induced plasticization phenomenon in glassy polymers for gas separation membrane. *Separation and Purification Technology, 27*(3), 173-194.

Jal, P. K., Patel, S., & Mishra, B. K. (2004). Chemical modification of silica surface by immobilization of functional groups for extractive concentration of metal ions. *Talanta, 62*(5), 1005-1028.

Jeong, H.-K., Nair, S., Vogt, T., Dickinson, L. C., & Tsapatsis, M. (2003). A highly crystalline layered silicate with three-dimensionally microporous layers. *Nat Mater, 2*(1), 53-58.

Kenarsari, S. D., Yang, D., Jiang, G., Zhang, S., Wang, J., Russell, A. G., Wei, Q., & Fan, M. (2013). Review of recent advances in carbon dioxide separation and capture. *Rsc Advances, 3*(45), 22739-22773.

Kentish, S. E. (2011). 11 - Polymeric membranes for natural gas processing. In A. Basile & S. P. Nunes (Eds.), *Advanced Membrane Science and Technology for Sustainable Energy and Environmental Applications* (pp. 339-360): Woodhead Publishing.

Khan, M. M., Filiz, V., Bengtson, G., Shishatskiy, S., Rahman, M., & Abetz, V. (2012). Functionalized carbon nanotubes mixed matrix membranes of polymers of intrinsic microporosity for gas separation. *Nanoscale Research Letters, 7*(1), 504-504.

Khulbe, K. C., Feng, C. Y., & Matsuura, T. (2007). *Synthetic Polymeric Membranes: Characterization by Atomic Force Microscopy*: Springer.

Kim, S., & Lee, Y. M. (2013). High performance polymer membranes for CO2 separation. *Current Opinion in Chemical Engineering, 2*(2), 238-244.

Kim, W.-g., Choi, S., & Nair, S. (2011). Swelling, Functionalization, and Structural Changes of the Nanoporous Layered Silicates AMH-3 and MCM-22. *Langmuir, 27*(12), 7892-7901.

Kim, W.-g., Lee, J. S., Bucknall, D. G., Koros, W. J., & Nair, S. (2013). Nanoporous layered silicate AMH-3/cellulose acetate nanocomposite membranes for gas separations. *Journal of Membrane Science, 441*(0), 129-136.

Kim, W.-g., & Nair, S. (2013). Membranes from nanoporous 1D and 2D materials: A review of opportunities, developments, and challenges. *Chemical Engineering Science, 104*(0), 908-924.

Koros, W. J. (2002). Gas separation membranes: needs for combined materials science and processing approaches. *Macromolecular Symposia, 188*(1), 13-22.

Koros, W. J., Vu, D. Q., Mahajan, R., & Miller, S. J. (2003). Mixed matrix membranes capable of separating carbon dioxide from mixtures including carbon dioxide and methane, and processes for purifying methane using the membranes, are disclosed. The membranes are polymer membranes with a: Google Patents.

Koyano, K. A., Tatsumi, T., Tanaka, Y., & Nakata, S. (1997). Stabilization of Mesoporous Molecular Sieves by Trimethylsilylation. *The Journal of Physical Chemistry B, 101*(46), 9436-9440.

Kumbharkar, S. C., Karadkar, P. B., & Kharul, U. K. (2006). Enhancement of gas permeation properties of polybenzimidazoles by systematic structure architecture. *Journal of Membrane Science, 286*(1–2), 161-169.

Lalia, B. S., Kochkodan, V., Hashaikeh, R., & Hilal, N. (2013). A review on membrane fabrication: Structure, properties and performance relationship. *Desalination, 326*(0), 77-95.

Lezcano, M., Ribotta, A., Miro, E., Lombardo, E., Petunchi, J., Moreaux, C., & Dereppe, J.-M. (1997). Spectroscopic characterization of dealuminated H-mordenites: The role of different aluminum species on the SCR of NO with methane. *Journal of Catalysis, 168*(2), 511-521.

Li, J.-R., Ma, Y., McCarthy, M. C., Sculley, J., Yu, J., Jeong, H.-K., Balbuena, P. B., & Zhou, H.-C. (2011). Carbon dioxide capture-related gas adsorption and separation in metal-organic frameworks. *Coordination Chemistry Reviews, 255*(15–16), 1791-1823.

Lin, Y.-H. (2003). Polymer viscoelasticity: basics, molecular theories, and experiments.

McKelvey, S. A., & Koros, W. J. (1996). Phase separation, vitrification, and the manifestation of macrovoids in polymeric asymmetric membranes. *Journal of Membrane Science, 112*(1), 29-39.

Morrow, B., & Gay, I. (2000). Infrared and NMR characterization of the silica surface. *Surfactant Science Series*, 9-34.

Nair, S., Chowdhuri, Z., Peral, I., Neumann, D. A., Dickinson, L. C., Tompsett, G., Jeong, H.-K., & Tsapatsis, M. (2005). Translational dynamics of water in a nanoporous layered silicate. *Physical Review B, 71*(10), 104301.

Noble, R. D. (2011). Perspectives on mixed matrix membranes. *Journal of Membrane Science, 378*(1–2), 393-397.

Othman, M. R., Tan, S. C., & Bhatia, S. (2009). Separability of carbon dioxide from methane using MFI zeolite–silica film deposited on gamma-alumina support. *Microporous and Mesoporous Materials, 121*(1–3), 138-144.

Pavlidou, S., & Papaspyrides, C. D. (2008). A review on polymer–layered silicate nanocomposites. *Progress in Polymer Science, 33*(12), 1119-1198.

Peng, N., Chung, T.-S., & Wang, K. Y. (2008). Macrovoid evolution and critical factors to form macrovoid-free hollow fiber membranes. *Journal of Membrane Science, 318*(1–2), 363-372.

Pinnau, I., & Koros, W. J. (1993). A qualitative skin layer formation mechanism for membranes made by dry/wet phase inversion. *Journal of Polymer Science Part B: Polymer Physics, 31*(4), 419-427.

Poling, B. E., Prausnitz, J. M., & O'Connell, J. P. (2001). *The properties of gases and liquids*: McGraw-Hill.

Rezakazemi, M., Ebadi Amooghin, A., Montazer-Rahmati, M. M., Ismail, A. F., & Matsuura, T. (2014). State-of-the-art membrane based CO2 separation using mixed matrix membranes (MMMs): An overview on current status and future directions. *Progress in Polymer Science, 39*(5), 817-861.

Robeson, L. M. (2008). The upper bound revisited. *Journal of Membrane Science, 320*(1–2), 390-400.

Rufford, T. E., Smart, S., Watson, G. C. Y., Graham, B. F., Boxall, J., Diniz da Costa, J. C., & May, E. F. (2012). The removal of CO2 and N2 from natural gas: A review of conventional and emerging process technologies. *Journal of Petroleum Science and Engineering, 94–95*(0), 123-154.

Sanders, D. F., Smith, Z. P., Guo, R., Robeson, L. M., McGrath, J. E., Paul, D. R., & Freeman, B. D. (2013). Energy-efficient polymeric gas separation membranes for a sustainable future: A review. *Polymer, 54*(18), 4729-4761.

Schmeling, N., Konietzny, R., Sieffert, D., Rölling, P., & Staudt, C. (2010). Functionalized copolyimide membranes for the separation of gaseous and liquid mixtures. *Beilstein Journal of Organic Chemistry, 6*, 789-800.

Scholes, C. A., Chen, G. Q., Stevens, G. W., & Kentish, S. E. (2010). Plasticization of ultra-thin polysulfone membranes by carbon dioxide. *Journal of Membrane Science, 346*(1), 208-214.

Shamsabadi, A. A., Kargari, A., Babaheidari, M. B., Laki, S., & Ajami, H. (2013). Role of critical concentration of PEI in NMP solutions on gas permeation characteristics of PEI gas separation membranes. *Journal of Industrial and Engineering Chemistry, 19*(2), 677-685.

Shimekit, B., & Mukhtar, H. (2012). Natural Gas Purification Technologies - Major Advances for CO2 Separation and Future Directions. In H. Al-Megren (Ed.), *Advances in Natural Gas Technology*: InTech.

Sing, K. S. W., Everett, D. H., Haul, R. A. W., Moscou, L., Pierotti, R. A., RouqueroL, J., & Siemieniewska, T. (1985). Reporting physisorption data for gas/solid systems, with special reference to the determination of surface area and porosity (recommendations 1984). *Pure and applied chemistry, 57*(4), 603-619.

Sridhar, S., Smitha, B., Mayor, S., Prathab, B., & Aminabhavi, T. M. (2007). Gas permeation properties of polyamide membrane prepared by interfacial polymerization. *Journal of Materials Science, 42*(22), 9392-9401.

Stern, S. (1968). The "Barrer" permeability unit. *Journal of Polymer Science Part A‐2: Polymer Physics, 6*(11), 1933-1934.

Takahashi, N., & Kuroda, K. (2011). Materials design of layered silicates through covalent modification of interlayer surfaces. *Journal of Materials Chemistry, 21*(38), 14336-14353.

Tsapatsis, M., Jeong, H. K., & Nair, S. (2005). Layered silicate material and applications of layered materials with porous layers: Google Patents.

Visser, T., Masetto, N., & Wessling, M. (2007). Materials dependence of mixed gas plasticization behavior in asymmetric membranes. *Journal of Membrane Science, 306*(1–2), 16-28.

Wijmans, J. G., & Baker, R. W. (1995). The solution-diffusion model: a review. *Journal of Membrane Science, 107*(1–2), 1-21.

Xu, G., Liang, F., Yang, Y., Hu, Y., Zhang, K., & Liu, W. (2014). An Improved CO2 Separation and Purification System Based on Cryogenic Separation and Distillation Theory. *Energies, 7*(5), 3484-3502.

Yampolskii, Y. (2011). 2 - Fundamental science of gas and vapour separation in polymeric membranes. In A. Basile & S. P. Nunes (Eds.), *Advanced Membrane Science and Technology for Sustainable Energy and Environmental Applications* (pp. 22-55): Woodhead Publishing.

Yeo, S.-D., Kang, I.-S., & Kiran, E. (2002). Critical polymer concentrations of polyethylene solutions in pentane. *Journal of Chemical & Engineering Data, 47*(3), 571-574.

Zhang, Y., Sunarso, J., Liu, S., & Wang, R. (2013). Current status and development of membranes for CO2/CH4 separation: A review. *International Journal of Greenhouse Gas Control, 12*(0), 84-107.

APPENDIX

Calculations

To calculate the volume and weight adjusted for a given weight percent

Fabrication of PSf membrane – 10mL dope solution of 23 wt.-% PSf and 77 wt.-% NMP

Density $_{PSf}$: 1.24g/mL

Density $_{NMP}$: 1.03g/mL

Taking 100 gram as basis

$$Volume\ _{PSf} = \frac{Weight_{PSf}}{Density_{PSf}} = \frac{23\ g}{1.24\ g/mL} = 18.55\ mL$$

$$Volume\ _{NMP} = \frac{Weight_{NMP}}{Density_{NMP}} = \frac{77\ g}{1.03\ g/mL} = 74.76\ mL$$

$$Volume\ _{PSf+NMP} = 18.55\ mL + 74.76\ mL = 93.31\ mL$$

$$Volume\ adjusted\ _{NMP} = Volume\ _{NMP} \times \frac{Volume_{dope\ solution}}{Volume_{PSf+NMP}}$$

$$= 74.76\ mL \times \frac{10\ mL}{93.31\ mL}$$

$$= 8.01\ mL$$

$$Volume\ adjusted\ _{PSf} = Volume\ _{PSf} \times \frac{Volume_{dope\ solution}}{Volume_{PSf+NMP}}$$

$$= 18.55\ mL \times \frac{10\ mL}{93.31\ mL}$$

$$= 1.99\ mL$$

$$Weight\ adjusted\ _{PSf} = \frac{Volume\ adjusted\ _{PSf}}{Density_{PSf}}$$

$$= 1.99\ mL \times 1.24\ g/mL$$

$$= 2.47\ g$$